Title

Evolutionary patterns of cat-like carnivorans unveil drivers of the sabertooth morphology

Journal

Current Biology, 34(11)

ISSN

0960-9822

Authors

Chatar, Narimane

Michaud, Margot

Tamagnini, Davide

et al.

Publication Date

2024-06-01

DOI

10.1016/j.cub.2024.04.055

Article

Current Biology

Evolutionary patterns of cat-like carnivorans unveil drivers of the sabertooth morphology

Highlights

- There is a continuous spectrum of cat-like phenotypes with sporadic convergence
- Saber-toothed taxa show reduced integration and high early evolutionary rates
- Disparity is high among sabertooths, yet cat-like carnivorans decline after the Miocene
- The emergence of large sabertooths appears to act as a macroevolutionary ratchet

Authors

Narimane Chatar, Margot Michaud, Davide Tamagnini, Valentin Fischer

Correspondence

narimane.chatar@berkeley.edu

In brief

Chatar et al. explore the tempo and mode of cat-like mammal evolution, highlighting a shape continuum from small cats to extreme sabertooths. They observe the highest disparities and evolutionary rates in clades with the most extreme sabertooth morphologies adaptations. These morphologies arose in clades with more plastic, less integrated skulls.

Chatar et al., 2024, Current Biology *34*, 1–14
June 3, 2024
https://doi.org/10.1016/j.cub.2024.04.055

CellPress

Please cite this article in press as: Chatar et al., Evolutionary patterns of cat-like carnivorans unveil drivers of the sabertooth morphology, Current Biology (2024), https://doi.org/10.1016/j.cub.2024.04.055

Current Biology

CellPress
OPEN ACCESS

Article

Evolutionary patterns of cat-like carnivorans unveil drivers of the sabertooth morphology

Narimane Chatar,[1,2,5,6,*] Margot Michaud,[1,3] Davide Tamagnini,[4] and Valentin Fischer[1]
[1]Evolution and Diversity Dynamics Lab, Université de Liège, Allée du six août 14, 4000 Liège, Belgium
[2]Functional Anatomy and Vertebrate Evolution Lab, Department of Integrative Biology, University of California, Berkeley, 3040 Valley Life Sciences Building, Berkeley, CA 94720, USA
[3]Département Formation et Recherche Sciences et Technologie, Université de Guyane, WMMX+5Q3, Cayenne 97300, Guyane
[4]Department of Biology and Biotechnologies, Sapienza University of Rome, Piazzale Aldo Moro 5, 00185 Roma, Italy
[5]X (formerly Twitter): @NarimaneChatar
[6]Lead contact
*Correspondence: narimane.chatar@berkeley.edu
https://doi.org/10.1016/j.cub.2024.04.055

SUMMARY

The sabertooth morphology stands as a classic case of convergence, manifesting recurrently across various vertebrate groups, prominently within two carnivorans clades: felids and nimravids. Nonetheless, the evolutionary mechanisms driving these recurring phenotypes remain insufficiently understood, lacking a robust phylogenetic and spatiotemporal framework. We reconstruct the tempo and mode of craniomandibular evolution of Felidae and Nimravidae and evaluate the strength of the dichotomy between conical and saber-toothed species, as well as within saber-toothed morphotypes. To do so, we investigate morphological variation, convergence, phenotypic integration, and evolutionary rates, employing a comprehensive dataset of nearly 200 3D models encompassing mandibles and crania from both extinct and extant feline-like carnivorans, spanning their entire evolutionary timeline. Our results reject the hypothesis of a distinctive sabertooth morphology, revealing instead a continuous spectrum of feline-like phenotypes in both the cranium and mandible, with sporadic instances of unequivocal convergence. Disparity peaked at the end of the Miocene and is usually higher in clades containing taxa with extreme sabertoothed adaptations. We show that taxa with saberteeth exhibit a lower degree of craniomandibular integration, allowing to exhibit a greater range of phenotypes. Those same groups usually show a burst of morphological evolutionary rate at the beginning of their evolutionary history. Consequently, we propose that a reduced degree of integration coupled with rapid evolutionary rates emerge as key components in the development of a sabertooth morphology in multiple clades.

INTRODUCTION

Felidae, a highly diverse carnivoran family, emerged during the Oligocene in Eurasia and quickly spread worldwide during the Miocene.[1] Although Felidae represents the sole extant cat-like clade, the sabertoothed morphotype is a textbook example of iterative evolution (sensu[2,3]), having evolved many times among placentals, marsupials, and gorgonopsians.[4–8] Nimravidae is a well-diversified yet fully extinct carnivoran clade that extensively explored a range of cat-like morphologies,[5] and although they have been commonly called "false cats" or "false sabertooth cats" in opposition to the "true cats," they evolved cat-like morphologies, including both saber-toothed and non-saber-toothed forms, tens of millions of years prior to the appearance of felids. Saber-toothed taxa are thought to feed on larger prey than similar-sized conical-toothed cats,[6,9–12] and a clear dichotomy between the craniomandibular shape of saber- and non-saber-toothed forms was expected based on this assumption. However, recent studies highlight that the functioning of the cat-like mandible[13,14] or even the shape[15] and functioning of the cat-like cranium[16] are more complex than previously expected. Even the assumption that saber-toothed taxa hunted significantly larger prey has been challenged, with some authors suggesting predation on species within a size range similar to those targeted by present-day carnivorans.[17] One possible implication of this emerging continuum of shape and function across saber-toothed and conical-toothed cats is that niche overlap between those two morphotypes might be stronger than previously thought, as first noted in Werdelin et al.[18]

Although previous studies already used morphometry to quantify the cranial or mandibular shape variations within cat-like carnivorans[15,19–23], little attention has been given to the spatiotemporal component of such variations, and the phylogenetic context is often overlooked; previous studies usually focused either on the cranium or the mandible. This hinders a comprehensive understanding of the cat-like feeding apparatus, leaving key questions unanswered: is there a clear dichotomy between morphotypes/clades and how does craniomandibular shape change over time and space and across clades? Can we identify times, clades, or places characterized by a particularly high or low disparity?

Please cite this article in press as: Chatar et al., Evolutionary patterns of cat-like carnivorans unveil drivers of the sabertooth morphology, Current Biology (2024), https://doi.org/10.1016/j.cub.2024.04.055

To answer these questions, we reconstruct the tempo and mode of craniomandibular evolution within Felidae and Nimravidae within a contemporary phylogenetic framework. We gathered a large-scale three-dimensional (3D) morphometric dataset (189 3D models) spanning the entire evolutionary histories of both clades, covering a total 36 million years of evolution (Data S1). Our hypothesis posits that cat-like carnivorans have been "shoehorned" into various categories/morphotypes over the years, while their craniomandibular shape exhibits a nuanced disparity beyond prior conceptions.

To test this hypothesis, we adopt two distinct methodological approaches. Initially, we employ a qualitative approach grounded in multivariate morphospaces. Then, we started to explore the tempo by depicting the disparity across time and space in the different clades. Subsequently, we transition to a quantitative approach, employing a battery of widely used statistical tests to characterize the evolutionary dynamics governing morphological evolution. Specifically, we evaluate the tempo of evolution by quantifying evolutionary rates, while exploring the mode of evolution involves assessing various factors such as the impact of phylogeny (phylogenetic signal) on craniomandibular morphological variation, the presence of constraints shaping evolutionary trajectories (phenotypic integration), and the occurrence of convergent evolution among taxa with similar phenotypes across different clades (C metrics[24] and theta tests[25]) as understanding the evolutionary context within which morphologies arise also requires knowledge of those constraints. Indeed, morphological modules (e.g., braincase, face, ascending ramus, mandibular corpus) evolving independently can lead to greater phenotypic disparity, whereas more integrated structures tend to constrain disparity.[26–33] Nevertheless, highly integrated structures can also lead to a substantial disparity through amplification of extreme phenotypes when evolving hand in hand in a multidimensional space.[34] Therefore, we analyzed the strength of modularity both within and across the cranium and the mandible in felids and nimravids as well as their rate of phenotypic evolution per branch. The hypothesis we test here is that conical and sabertooth clades have distinct patterns of integration.

RESULTS

Morphospaces occupation, convergence, and global disparity

Global morphospace occupation of cat-like carnivorans (Figure 1; see Data S1A and S1D for the list of specimens used in those analyses; Figure S1 for the landmarks placed; Figure S2 for annotated morphospace with taxa names and back transform morphospace) do not show a clear subdivision between sabretooth and non-sabretooth taxa, although our cluster dendrograms retrieved a marked dichotomy separating both extreme morphotypes by a quite long branch length, even retrieving significant p values between the two groups (p = 0.000999 for both the skull and the mandible datasets) (Figure S3 for tanglegrams comparing phylogeny and cluster based on 3D data). Instead, for the mandibles (Figure 1A), morphospace occupation shows a clear continuum of shape from the small felines (*Felis* spp., *Prionailurus* spp., *Leopardus* spp., *Caracal* spp., etc.), with a curved mandibular body, short diastema, and a high coronoid process projected dorsally, to the most extreme saber-toothed taxa (*Barbourofelis* spp.), with a short and straight coronoid process, long diastema, and the development of a mandibular flange. The peak showing the densest occupation in the morphospace is shared between middle- and large-sized felines (*Panthera* spp., *Lynx* spp., *Pseudaelurus* spp., etc.), metailurins (*Yoshi* spp., *Metailurus* spp.), and early machairodontines (*Paramachairodus* spp., *Promegantereon ogygia*, and *Machairodus aphanistus*), seemingly reflecting the most recurring shape in the evolution of cat-like carnivorans.

This is also the case when looking at cranium shape (Figure 1B), with a continuum of shape in between middle- and large-sized felines, plus extreme saber-toothed taxa. However, in this case, small felines form a second peak of recurrent morphology separated from their larger counterparts by a valley of uncommon phenotypes. In this region of the morphospace, which is less densely populated, we still encounter the cheetah, *Acinonyx jubatus*, alongside certain fossil taxa, including *Machairodus aphanistus*, *Yoshi minor*, *Yoshi garevski*, and *Paramachaerodus maximiliani*. Some small saber-toothed taxa (e.g., *Yoshi minor*) are quite close to that peak. Extreme saber-toothed taxa are more scattered in our morphospace as they do not form a peak of recurring morphology. Although the most derived nimravids occupied regions in both morphospace that were never reached by felids (high PC1 on both Figures 1A and 1B), felids also have their own morphological innovation. Indeed, a small feline morphotype (taxa weighing only a few kilograms: *Felis* spp., *Prionailurus* spp., *Leopardus* spp., etc. with a really rounded skull) never occurred in nimravids or even in machairodontine felids. Allometry is strong enough in the dataset so that we retrieved a significant p value in our procD.lm test for the mandible (0.001) but is less marked in the cranium, resulting in a non-significant p value (0.086).

To test the strength of craniomandibular convergence, we used two different metrics designed to detect the occurrence of retained and/or evolved similarity. Stayton's C1 is a distance-based measure quantifying how far two or more taxa have evolved to be more similar to one another than their ancestors were to each other, ranging from 0 (no convergence) to 1 (complete convergence leading to the same morphology).[24] The θ angle, on the other hand, represents the angle between phenotypic vectors and span from 0° (very similar phenotypes) to 180° (very dissimilar phenotype).[25] Although C metrics are found significant only in the case of convergence, Castiglione θ can be found significant both in the presence of convergence and conservatism; combining those two metrics in the same study therefore allows researchers to untangle those two evolutionary trends. More details about those convergence metrics are available in the STAR Methods section. Surprisingly, extremely few tested pairs were found to be significantly convergent according to the metrics used (Tables 1 and S3; Figures S2G and S2H). None of the tested pairs was found significant for both Stayton C1 and Castiglione θ questioning the potential convergence between those pairs. Also, for the three taxa pairs providing significant results, only one of the structures (either the cranium of the mandible) showed some degree of convergence. *Yoshi minor* and *Acinonyx jubatus*, although showing striking resemblances in the cranial shape (Figures 1B and S2H), were convergent only regarding their mandibular shape according to the Stayton C metrics. Stayton metrics

Please cite this article in press as: Chatar et al., Evolutionary patterns of cat-like carnivorans unveil drivers of the sabertooth morphology, Current Biology (2024), https://doi.org/10.1016/j.cub.2024.04.055

CellPress
OPEN ACCESS

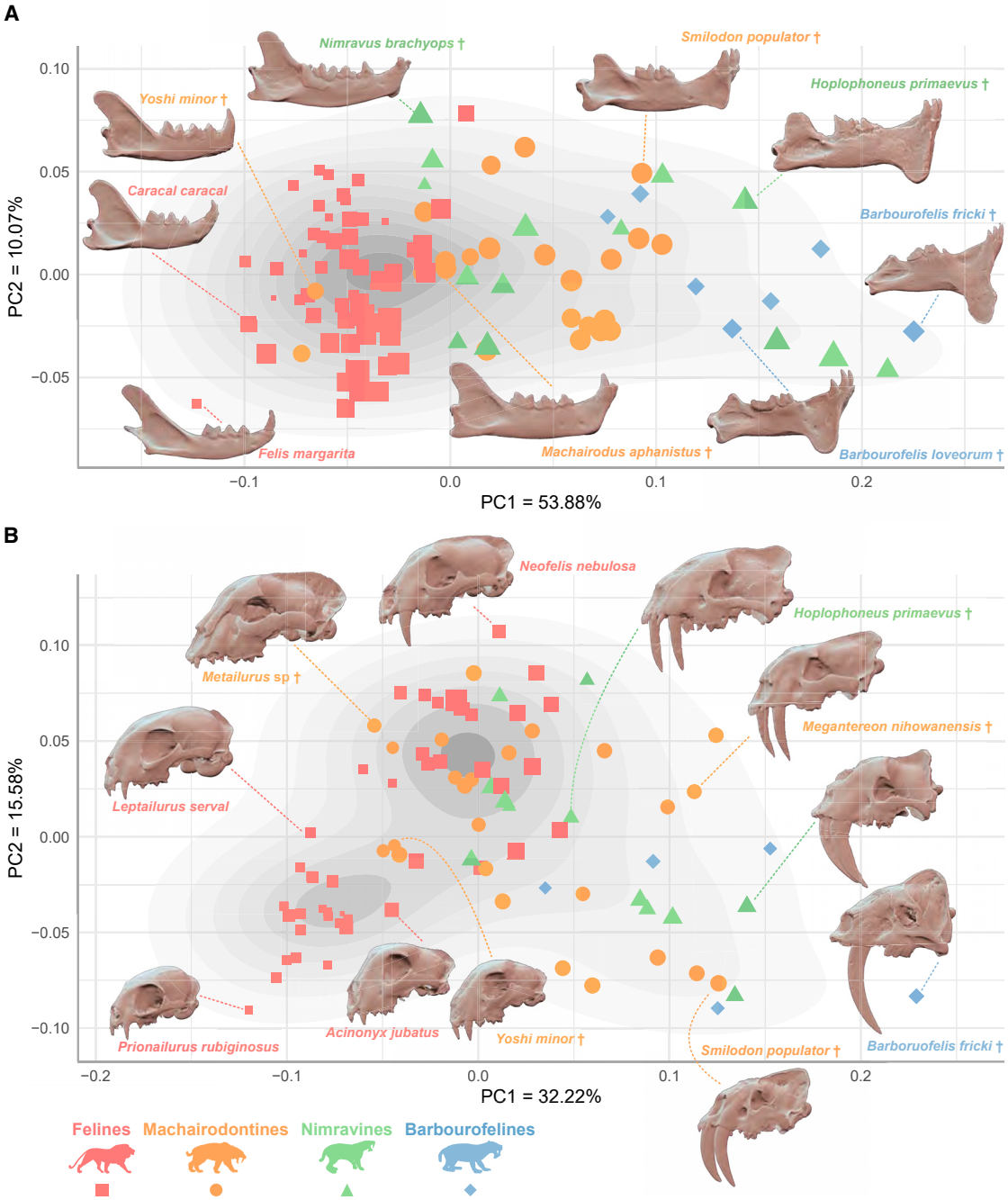

Figure 1. Morphospace occupation

Morphospace occupation of cat-like carnivorans for the mandible (A) and the skull (B). Point size was set relative to the log of the centroid size. See Figure S2 for backtransfrom shapes and annotated morphospaces with species names. Gray shading represents morphospace occupation density, and every point represents a specimen from Data S1A and S1B.

also retrieved the pair *Megantereon nihowanensis* and *Eusmilus adelos* to be significantly convergent, while Castiglione θ highlighted convergence or conservatism in the cranium of *Neofelis nebulosa* and *Nimravus brachyops* as well as the mandible of *Neofelis nebulosa* and *Metailurus major*. Although the clouded leopard was sometimes presented as an example of convergence[35–37] with machairodontine felids, it was never compared with nimravids. However, it is clear from Figures 1A and S9A that in this case the clouded leopard does not particularly show a saber-tooth-like craniomandibular shape, whereas *Nimravus brachyops* and *Metailurus major* exhibit an incredibly feline-like craniomandibular shape, falling close to extant felines in the morphospace, very close to the oldest felid, *Proailurus lemanensis*. Also, since only the Castiglione θ was found to be

Please cite this article in press as: Chatar et al., Evolutionary patterns of cat-like carnivorans unveil drivers of the sabertooth morphology, Current Biology (2024), https://doi.org/10.1016/j.cub.2024.04.055

Table 1. Results of the convergence tests using the Stayton C1 and Castiglione θ

Pairs	Bone	Stayton[24]		Castiglione et al.[25]			
		C1 Stayton	*p* value C1	Theta (θ)	*p* value θ	Time corr. θ	*p* value T corr. θ
Yoshi minor-Acinonyx jubatus	cranium	0.011	0.530	11.211	0.709	0.162	0.711
	mandible	0.398[a]	0.029[a]	4.881	0.176	0.060	0.088
Hoplophoneus primaevus-Homotherium serum	cranium	0	1	9.395	0.475	0.118	0.351
	mandible	0.037	0.469	6.19	0.112	0.149	0.412
Machairodus aphanistus-Panthera pardus	cranium	0	1	8.118	0.320	0.111	0.292
	mandible	0.033	0.461	6.198	0.382	0.149	0.382
Megantereon nihowanensis-Eusmilus adelos	cranium	0.342[a]	0.03[a]	8.007	0.320	0.098	0.177
Megantereon cultridens-Eusmilus sicarius	mandible	0.158	0.192	9.848	0.791	0.214	0.686
Neofelis nebulosa-Nimravus brachyops	cranium	0.001	0.611	7.329	0.205	0.087[a]	0.050[a]
	mandible	0.034	0.535	6.882	0.513	0.274	0.513
Neofelis nebuolsa-Metailurus major	cranium	0.037	0.383	7.749	0.252	0.112	0.209
	mandible	0.247	0.102	4.987	0.295	0.0087[a]	0.049[a]
Machairodus aphanistus-Nimravus brachyops	cranium	0	1	10.004	0.581	0.131	0.482
	mandible	0	1	6.460	0.408	0.155	0.418

C2–C4 can be found in Table S3; see Figures S2G and S2H for a more visual interpretation.
[a]Significant *p* values.

significant in this case while Stayton C1 was not, the resemblance between *Neofelis nebulosa* and *Nimravus brachyops* is likely the result of conservatism.

The highest disparity is observed in nimravines for the mandible and machairodontine felids for the cranium, being somewhat comparable to that of barbourofelines (Figure S4). The disparity is globally greater in nimravids than in felids. This is unsurprising considering the co-existence of extreme sabretooth taxa such as *Barbourofelis* spp. with more feline-like taxa such as *Eofelis* spp. in this group.

Spatiotemporal patterns

During the Paleogene, nimravids already exhibit a wide continuum of cranial shapes, spanning from the average cat-like shapes to some more extreme saber-toothed forms (Figures 3 and S5), while their mandibular shape appears more far from the peak of recurring morphology (Figure 3). From the Miocene to the Pliocene, there is a wide distribution of specimens across our morphospace. However, in the Pleistocene, there was a pronounced divergence between machairodontine felids and felines sensu lato in terms of mandibular shape, with machairodontine felids consistently occupying more extreme regions of the morphospace, a pattern that is no retrieved for the cranial morphology. This differentiation is particularly noticeable in North America, where Pleistocene machairodontine (such as *Smilodon* spp., *Homotherium* spp., and *Xenosmilus hodsonae*) exhibit cranial shapes relatively similar to large cats in our dataset but display more extreme mandibular shapes (Figures 3 and S5). Cat-like carnivorans reached the area of recuring mandibular morphology during the Miocene and more precisely at the end of this Epoch (Figures 2, S4C, and S4D; Figure 3 for the occupation of morphospace through time and space for the mandible; Figure S5 for the cranium). From this Epoch, some taxa (i.e., extreme sabertooths and small felines) explored some unusual areas in the morphospace, but the area of recuring shape was always occupied (Figures 2, 3, S4, and S5). Although similar regions of the morphospace were occupied by taxa from separate clades during the Miocene and Pliocene (i.e., felines and primitive machairodontines/metailurines), those morphologically similar taxa were usually quite well distributed worldwide, although the Miocene in Asia and North America saw highly convergent felines and machairodontines: *Yoshi minor*/*Felis* sp. Indet in Asia and *Machairodus catacopis*/*Pseudaelurus* spp. In North America. However, the size differences within those co-existing taxa pairs during the Miocene probably facilitated cohabitation just like in extant taxa, such as leopards and tigers in Asia.[38,39] The peak of disparity in cat-like carnivorans is observed in the Late Miocene with the co-existence of barbourofelines and felids. The pattern of evolution of disparity through time is similar for both the cranium and mandible with a peak during the Miocene and a slow decline ever since. Although the disparity appears particularly low prior to the Miocene, this might be induced by a sampling bias despite bootstrapping, since a different pattern is visible in phylogenetically informed disparity Figures S4E–S4I). Please note that our dataset currently exhibits bias toward European and North American specimens, and further sampling is necessary to comprehensively grasp the spatiotemporal trends in craniomandibular shape among cat-like carnivorans. Specifically, more specimens from Asia and Africa are needed to provide a deeper understanding, and we encourage future studies along these lines.

Patterns of phenotypic integration, rates of evolution, and phylogenetic signal

Overall, there is a significant phylogenetic signal in almost all groups tested, except for the cranium of nimravids, nimravines, or in the cranium and mandible of barbourofelines (Table S4). The high K values emerging from those tests might suggest that the low sample size in nimravines and barbourofelines potentially plays in reducing statistical power.

Please cite this article in press as: Chatar et al., Evolutionary patterns of cat-like carnivorans unveil drivers of the sabertooth morphology, Current Biology (2024), https://doi.org/10.1016/j.cub.2024.04.055

CellPress
OPEN ACCESS

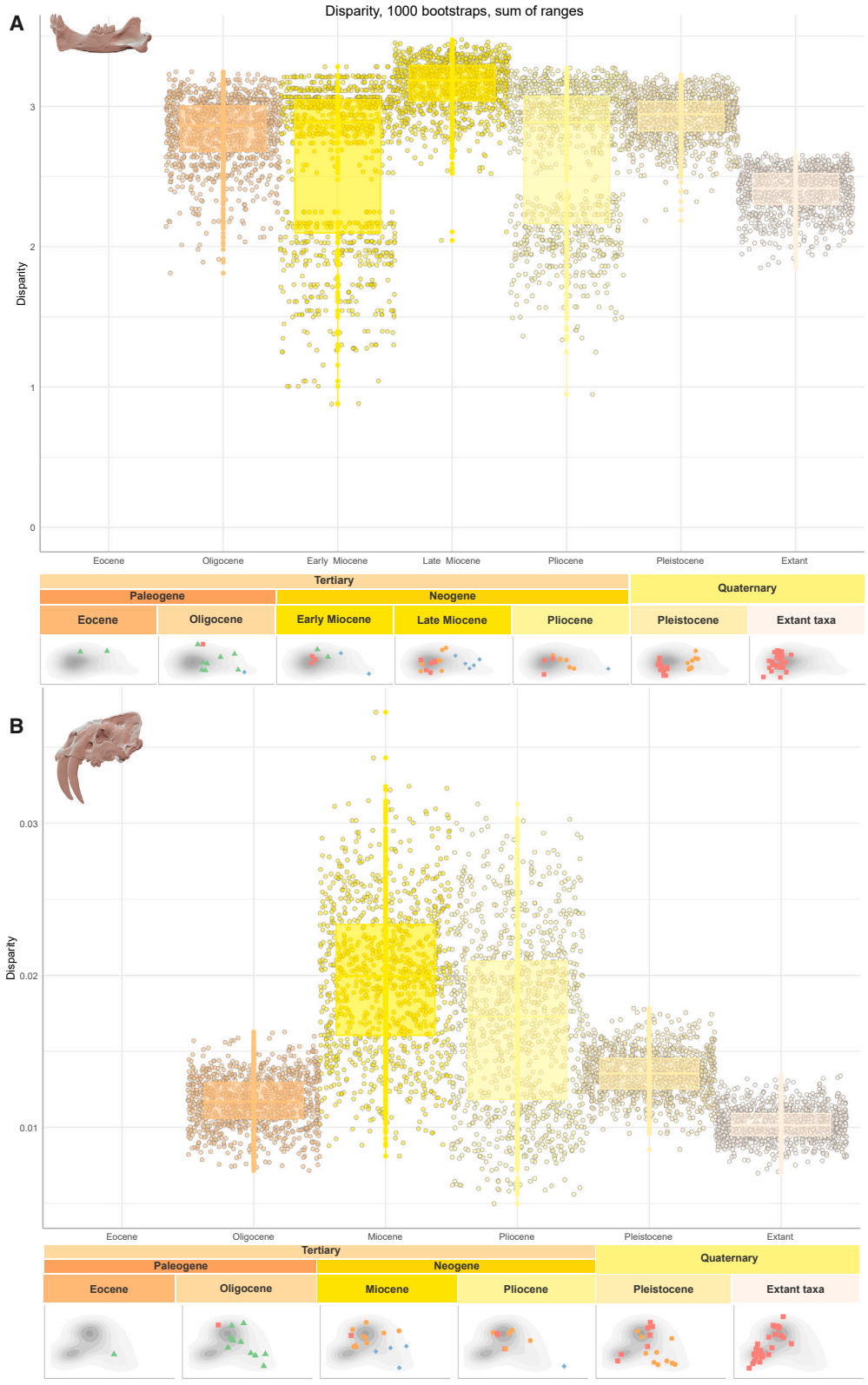

(legend on next page)

Please cite this article in press as: Chatar et al., Evolutionary patterns of cat-like carnivorans unveil drivers of the sabertooth morphology, Current Biology (2024), https://doi.org/10.1016/j.cub.2024.04.055

Also, our tanglegrams showing the results of our clustering analyses on the Procrustes coordinates against the phylogeny from the super tree (Figure S3) show no correspondences between phylogenetic relationships and craniomandibular shape in cat-like carnivorans unlike what is observed in the skull of extant carnivorans where some correspondences are still present in the cranium (see Law et al.[40]), which suggests a high degree of homoplasy in the dataset. This is consistent with the continuum of shape described earlier. Our analyses retrieved different patterns of morphological integration between the different cat-like clades (Figure 4). Overall, the integration between the cranium and the mandible is present in all groups except machairodontines. Felinae shows the highest degree of morphological integration between the tested structures. Almost all clades show a significant phenotypic integration between the anterior and posterior portion of each structure except barbourofelines for which the mandible does not show any significant integration between its corpus and ramus. Although felines show a high degree of integration between the anterior portion of the cranium and the anterior portion of the mandible, as well as the posterior section of the cranium and posterior section of the mandible, those covariations are not found in any of the other groups. In felines, the anterior portion of the mandible even covaries with the posterior portion of the cranium, and this is the only group in our dataset showing this degree of integration. Still, due to the relatively low sample size for certain clades, particularly nimravines and barbourofelines, these results should be interpreted with caution. They should be viewed as an initial exploratory step toward understanding patterns of phenotypic integration in cat-like carnivorans.

Our branch-specific rate of morphological evolution (Figure 5 for the mandible; Figure S6 for the cranium) highlighted a rapid burst at the beginning of the nimravid evolutionary history. Some lineages of small felines (*Prionailurus* spp.) also show a higher rate of morphological evolution than their larger counterparts, and this pattern is more marked for the cranium (Figure S6) than for the mandible (Figure 5). There are also many acceleration phases during the evolutionary history of machairodontine felids, especially in branches reaching *Smilodon* spp. And *Homotherium* spp. Except for some small taxa, as mentioned above, the rate is relatively stable and lower in felines. Branch-specific rates of morphological evolution remain relatively higher in nimravid compared with felids.

DISCUSSION

A continuum of shapes in cat-like carnivorans

Cat-like carnivorans have historically been classified using various dichotomies, such as true vs. false cats,[41–43] scimitar vs. dirk-toothed cats,[10,16,44,45] saber-toothed vs. non-saber-toothed cats,[6,46] primitive vs. derived sabertooth,[47,48] among others. However, our comprehensive morphospace analysis reveals a broad continuum of shapes (Figures 1, S2, and S3). This observation aligns with previous morphometric studies that have shown that cat-like carnivorans evolved relatively conservative morphologies within distinct clades.[15,19–21] Furthermore, recent research has highlighted the unexpected functional complexity within these taxa.[13,14,16] Some taxa considered as "primitive" machairodontine felids (e.g., *Paramachairodus* spp., *Promeganteron ogygia*, and *Machairodus aphanistus*), metailurins (*Yoshi* spp. and *Metailurus* spp.), or nimravids (e.g., *Eofelis*), or even some "derived" scimitar toothed, exhibit cranial shapes remarkably similar to those of pantherins and other large-bodied felines, although more differences can be found in the mandible (Figure 1). While it has been argued that *Paramachairodus* spp., *Promeganteron ogygia*, and *Machairodus aphanistus* exhibit clear machairodontinae characters[48–50] and that those primitive taxa must have used the same killing bite as their more derived counterparts,[11,51] their craniomandibular shapes (Figures 1, S2, S3, and S5) and the functioning of their mandible[14] suggest that they likely employed a different killing bite compared with *Smilodon* or even *Homotherium*. Our understanding of both the killing bite and hunting strategies employed by extinct cats remains limited. Throat and/or muzzle clamping in extant big cats would have been exceedingly challenging to predict using bone morphology alone. Furthermore, the concepts of the killing bite and hunting strategy represent distinct facets of prey acquisition, potentially evolving independently. Thus, understanding the precise methods by which extinct saber-toothed cats acquired their prey remains an ongoing challenge, likely without a definitive resolution.

Furthermore, nimravids, often labeled as false cats or sometimes "paleofelid" appeared long before felids[52,53] and exhibited a greater range of morphological diversity (Figures 3, 4, and S5) spanning nearly every region of the cat-like morphospace occupation, except for the small feline cranial morphotype (Figure 1B). Notably, nimravids produced some of the most extreme craniomandibular phenotypes among saber-toothed carnivorans, exemplified by the genus *Barbourofelis* (Figure 1). The distinction between false cats and true cats can be traced back to the earliest descriptions of nimravid remains by Cope, who extensively noted the similarities between nimravids and felids and even remarked, "[…] *As nothing but the characters of the canine teeth distinguished these from the typical feline […]*"[42] However, subsequent authors argued that nimravids constituted a distinct clade[54] relegating this group to the status of false cats, despite being truly the first cats to have appeared on Earth.

In conclusion, our analyses reveal a continuous spectrum of shape variation, where primitive machairodontine felids, metailurins, primitive nimravids, and certain derived scimitar-toothed cats closely resemble pantherins and other large-bodied felines in terms of cranial shape. However, notable differences emerge in the mandible, underlining the intricate disparity within this group.

Convergence and competition in cat-like carnivorans

The results of our convergence tests (Tables 1 and S3; Figures S2G and S2H) did not provide statistical evidence for convergence, in contrast to some previous studies that found

Figure 2. Disparity through time

Disparity through time computed as a sum of ranges in (A) the cat-like mandible and (B) the cat-like cranium, with occupation of the morphospace at each Epoch. The Miocene was divided into two time bins for the mandible dataset due to the great number of Miocene specimens (see STAR Methods for details). See Figure S4 for other metrics, disparity in every clade, and phylogenetic inferred disparity and Data S1 for specimens used as well as the FAD and LAD (first and last appearance datum, respectively) used to calibrate the supertree.

Please cite this article in press as: Chatar et al., Evolutionary patterns of cat-like carnivorans unveil drivers of the sabertooth morphology, Current Biology (2024), https://doi.org/10.1016/j.cub.2024.04.055

CellPress
OPEN ACCESS

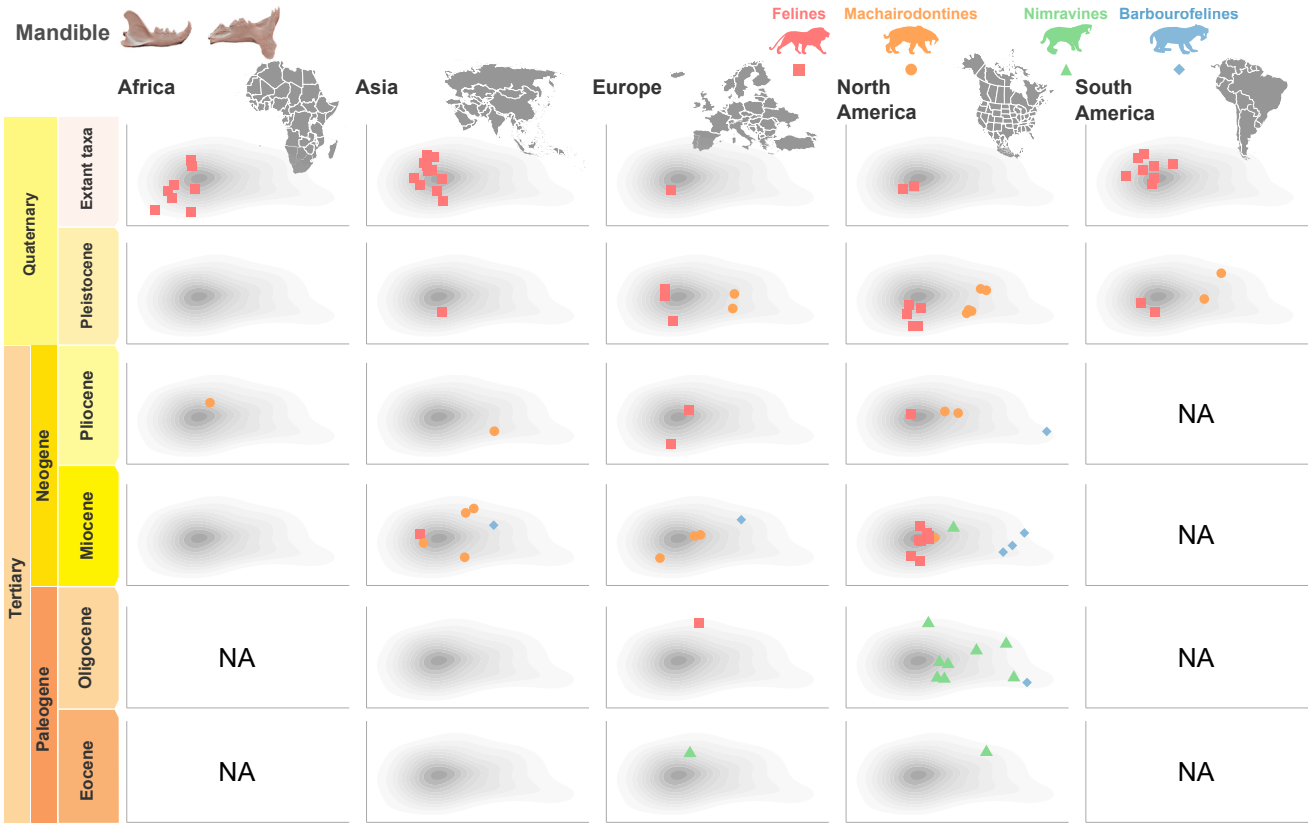

Figure 3. Occupation of the morphospace trough time and space for the mandible dataset
See Figure S5 for the cranium. See also Data S1A and S1B for the age and locality of each specimen.

statistically significant results at the family level.[55] It is essential to consider the methodology used in these tests: Stayton's metrics rely on the maximum phenotypic distance between ancestors, whereas Castiglione's method also takes into account the time since cladogenetic divergence. Given the relatively short divergence time among the studied taxa, this could explain the lack of significance in the Castigli'ne tests. Furthermore, the overall conservative morphology within these groups may result in a low maximum phenotypic distance between lineages at various points in their evolutionary histories (Dmax), impacting the results concerning Stayton's metrics.

Nevertheless, our cluster dendrogram still emphasizes the substantial craniomandibular similarities between some taxa in both families. This suggests that cranial shape closely follows clade-based evolutionary shifts, with cluster dendrograms effectively reflecting the distinctions between different families. However, mandibular shape evolution appears to be more influenced by other factors and does not consistently align with these phylogenetic relationships.[40] In our cluster dendrograms, we identified two distinct groups for both crania and mandibles: one comprising taxa with the shortest upper canines and another containing taxa with the longest upper canines (Figure S3) with a mixture of felids and nimravids found within each group. Despite the apparent cranial similarities, there exists a well-structured spatial and temporal distribution of these morphologically analogous taxa. This arrangement minimizes potential competition between morphologically similar species belonging to distinct clades, akin to the highly structured small felid guild observed in contemporary ecosystems, which acts to reduce competition.[56]

From an evolutionary perspective, small extant felines are as much derived as extreme sabertooth taxa

Small cat species, particularly in terms of cranial shape, form a second peak of recurring phenotypes. This demonstrates a deviation from the average/most common cat-like shape, comparable to the extremes seen in saber-toothed taxa like *Barbourofelis* spp. The small felines skull shape is characterized by a domed cranium, wide orbits with both postorbital processes nearly touching, a short and weak sagittal crest, and a low nuchal crest (Figure 1B). These morphological variations stand in stark contrast to the extreme saber-toothed carnivorans, such as *Barbourofelis fricki*, which display features like the rostrocaudal shortening of the sagittal crest and temporal fossa, the rotation of the occipital plane, and completely closed orbits, among others. Despite the differences, small felines find themselves equally distant from the main peak of recurring morphology, much like the extreme sabertooths. When considering both their mandibles and crania, it becomes evident that small felines are just as evolutionarily derived as the most extreme saber-toothed taxa and are equally distant from the earliest condition seen in the first felid, *Proailurus lemanensis*.[57,58] Small cats are well separated from larger taxa by an area of uncommon phenotype

Please cite this article in press as: Chatar et al., Evolutionary patterns of cat-like carnivorans unveil drivers of the sabertooth morphology, Current Biology (2024), https://doi.org/10.1016/j.cub.2024.04.055

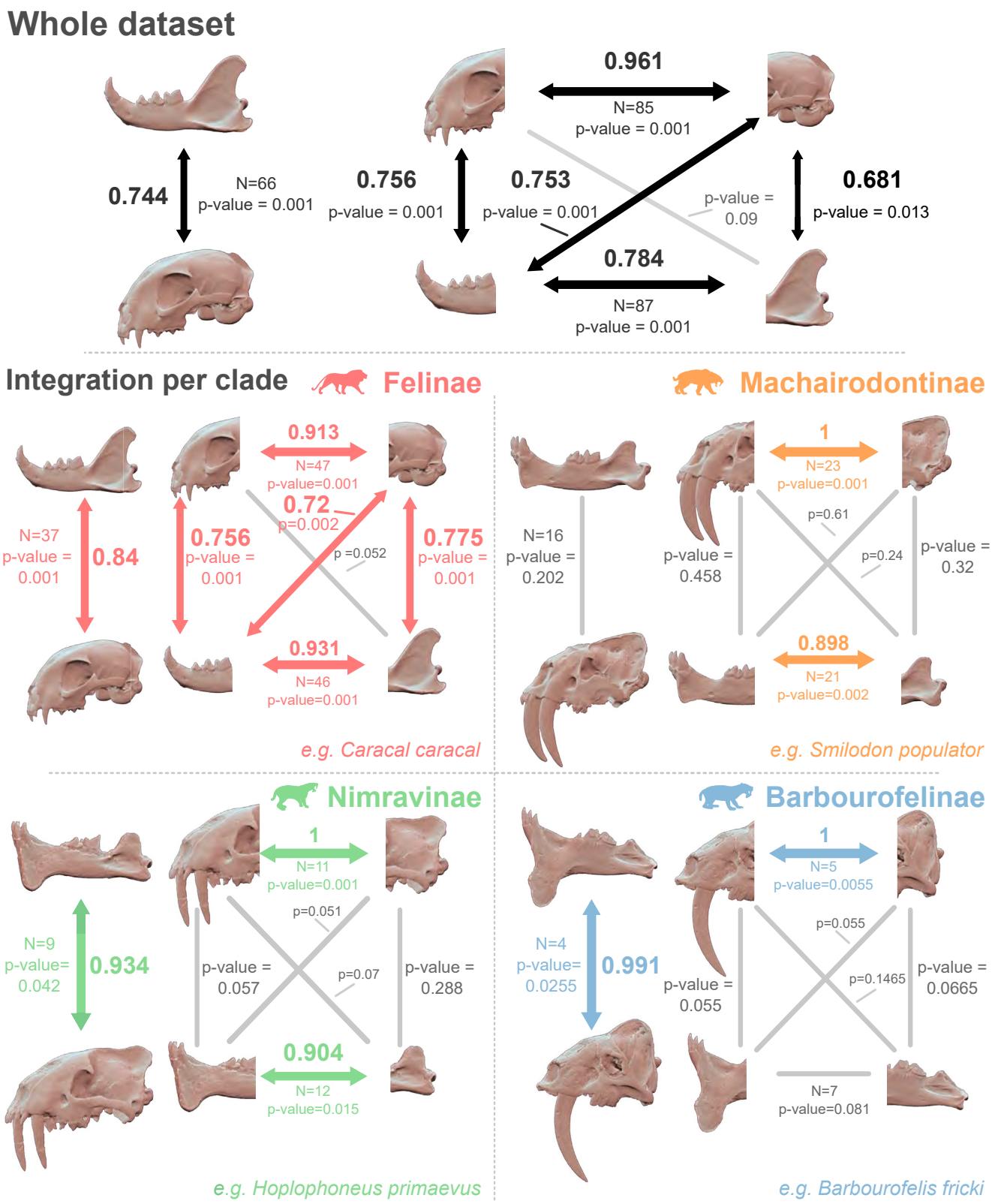

Figure 4. Phylogenetic integration tests

Line thickness depends on the r-partial least squares (PLS) values (indicated in bold next to each arrow as well as number of individuals *n* and *p* values). Gray lines without arrows indicate non-significant integration (*p* value > 0.05). See Data S1C and S1F for FAD and LAD used to calibrate the supertree.

Please cite this article in press as: Chatar et al., Evolutionary patterns of cat-like carnivorans unveil drivers of the sabertooth morphology, Current Biology (2024), https://doi.org/10.1016/j.cub.2024.04.055

CellPress
OPEN ACCESS

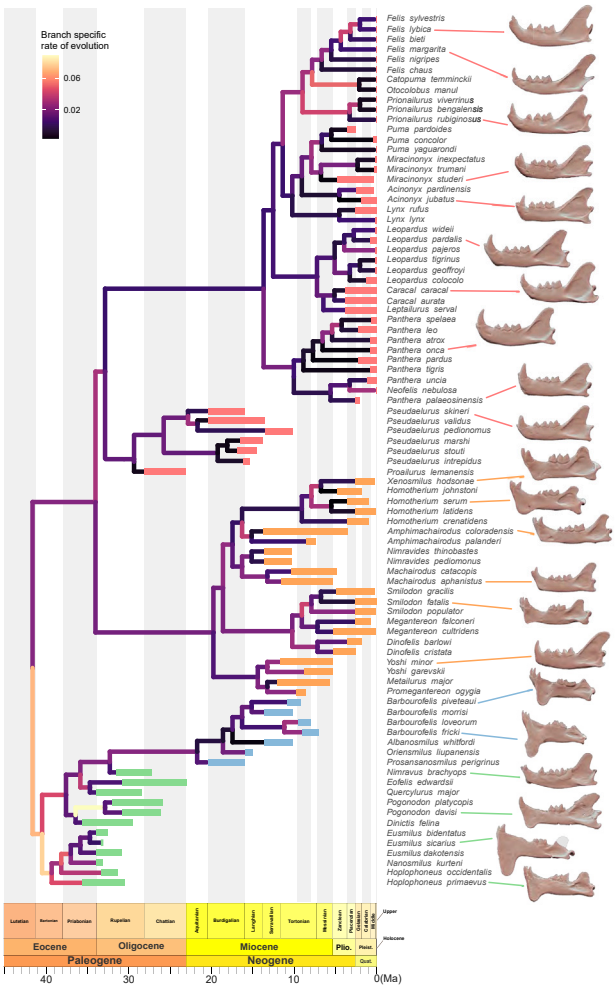

Figure 5. Branch-specific rate of morphological evolution for the mandible obtained from the RRPhylo function

Plio, Pliocene; Pleist, Pleistocene; and Quat, Quaternary. See Figure S6 for the cranium. See Data S1C and S1F for FAD and LAD used to calibrate the supertree and STAR Methods for details.

which could be due to a functional constraint linked to the strong difference in prey size with big cats hunting prey much larger than them while smaller cats tend to hunt preys only a fraction of their body weight.

Interestingly, the small feline morphotype never occurred in nimravids and appeared quite recently in the fossil record (during the Pleistocene; see Figures S4 and S5). However, this observation should be approached cautiously, as it could be influenced by fossilization biases. In modern ecosystems, small cats primarily inhabit densely forested areas like jungles or even deserts,[59] which may reduce their chances of fossilization.[60] Additionally, their smaller size results in thinner and more fragile bones, making them less likely to be preserved over geological time scales.[61]

Cat-like carnivorans are on the decline since the Miocene

Despite showcasing a unique morphological innovation, the distinctive small morphotype, felids have, over time, become confined to a considerably reduced area within the cat-like morphospace. This restriction has led to a significant loss in disparity, especially following the extinction of the machairodontine felids during the Late Pleistocene (Figures 2, 3, S4, and S5). Cat-like carnivorans reached their maximum disparity during the Miocene and, more precisely, at the end of the Miocene, characterized by the co-existence of extreme saber-toothed taxa and those with more feline-like characteristics. During this period, felids underwent substantial diversification.[18] Although nimravids were already on the decline[54] the simultaneous presence of the first felids and the last nimravids resulted in a wide array of shapes among cat-like carnivorans.

The evolution of cranial and mandibular shape through time and space also reveals different patterns for each bone. Although the first nimravids quickly exhibited a cranial shape relatively close to the most recurring cat-like shape, their mandibles appeared more extreme. The Pleistocene witnessed a marked divergence between machairodontines and felines, with machairodontines exhibiting heavily derived saber-toothed forms that departed significantly from the average cat-like shape (Figures 2 and 3) in terms of mandibular shape. However, their cranial shape remained much more similar to large felines s.l. from the same Epoch. Machairodontinae were often cited as an example of over-specialization, making them unable to adapt to changing ecosystems and potentially contributing to their own extinction.[62] Recently, Piras et al. found a higher extinction rate in saber-toothed taxa, attributing this pattern to a narrower ecological niche and less ecological flexibility.[21] Although machairodontine felids displayed considerable diversity[1,62,63] they ultimately succumbed to the various environmental shifts and faunal turnovers of the Late Pleistocene, vanishing alongside the rest of the megafauna.[64]

However, our analyses reveal that despite the apparent diversity, machairodontine felids rapidly moved away from the most common cat-like morphology, with extreme saber-toothed taxa occupying more highly specialized niches by the Pliocene. These findings contrast with those of Romano,[22] who observed a continuous increase in disparity among machairodontine felids, peaking during the Pleistocene. However, this discrepancy may be attributed to the limited number of taxa (17) and the use of a cladistic matrix from Christiansen,[63] which relies on character data rather than actual shape data. Although some authors support the use of cladistic data for characterizing disparity[65–67] caution must be exercised when interpreting such results from matrices with limited characters and taxa. Romano[22] interpreted this constant increase in morphospace as a "late saturation" (sensu[68]). Nevertheless, with a more extensive dataset, it becomes evident that machairodontine felids, and cat-like carnivorans in general, had been experiencing a decline in disparity long before their eventual extinction. Despite the repeated evolution of large saber-toothed forms, this morphological specialization seems to act as a macroevolutionary ratchet ultimately causing the decline of those lineages, as previously suggested in other studies.[69]

Could a lower degree of phenotypic integration and a higher rate morphological evolution be potential drivers of the sabretooth morphology?

When examining the skull as a single unit, cranial shape appears to be more constrained by allometry in taxa with short upper

Please cite this article in press as: Chatar et al., Evolutionary patterns of cat-like carnivorans unveil drivers of the sabertooth morphology, Current Biology (2024), https://doi.org/10.1016/j.cub.2024.04.055

canines, while in taxa with elongated upper canines, it is more related to the length of these canines.[15] Although not discussed as integration, Emerson and Radinsky[6] already started to introduce the covariation between the coronoid process and other typical sabertooth traits. Later, Meloro and Slater[70] have highlighted distinct patterns of integration between the anterior (face) and posterior (braincase) portions of the cranium, these two modules being driven by body size in taxa with short upper canines while relative canine length appears to drive rostrum shape in saber-toothed taxa. More recently, Tamagnini et al.[71] showed that extreme sabertooth adaptations of machairodontine break the craniofacial evolutionary allometry rule within felids. Similarly, Piras et al.[20] conducted integration tests on the cat-like mandible in their 2D geometric morphometric analyses, testing the hypothesis that sabertooth morphology entails covariation between the ascending ramus and the mandibular corpus.

In this contribution, we assessed integration degree between different subunits exploring new combinations, revealing that Felinae sensu lato is the clade with the highest degree of integration. This contrasts with the findings of Piras et al. who identified Barbourofelinae as the clade with the highest degree of integration, followed by Nimravinae, Machairodontinae, and Felinae, confirming their hypothesis. Saber-toothed taxa exhibit a wide range of morphologies within the same clade. For instance, within machairodontine felids, a similar reduction of the coronoid process can be associated with various degrees of development of a mandibular flange (see *Smilodon* spp., *Homotherium* spp., and *Megantereon* spp. or the development of the mandibular flange in *Barbourofelis* spp.; see Figure 1). Therefore, it is logical to assume that sabertooths have a lower degree of integration between the mandibular corpus and ramus to allow for such a wide range of possible combinations. By contrast, felines exhibit a more integrated morphology, with smaller taxa featuring slender and curved mandibular rami with a long and more posteriorly projected coronoid process, while larger taxa display a more robust corpus with a shorter and straighter coronoid process. It is the principle of morphological integration: if modules answer to different constraints, evolving independently, this eventually leads to a greater disparity, while more integrated structures tend to constraint phenotypic diversity.[26–33] The greater disparity observed in clades with longer upper canines (Figures 1 and S4) further supports the idea of a lower degree of integration in these groups. This lower degree of integration might even represent the initial step that allowed some cat-like carnivorans to develop sabertooth morphologies. This reduced integration, coupled with bursts in the rates of morphological evolution during sabertooth diversification, appears to have played a pivotal role in shaping the diversity of cat-like carnivorans.

STAR★METHODS

Detailed methods are provided in the online version of this paper and include the following:

SUPPLEMENTAL INFORMATION

Supplemental information can be found online at https://doi.org/10.1016/j.cub.2024.04.055.

ACKNOWLEDGMENTS

We are extremely thankful to all curators, collection managers, and staff, whose help and support were fundamental to collect all the scans we needed to perform this study. Especially, we would like to thank: Geraldine Véron and Guillaume Billet (MNHN, Paris, France), Daniela Kalthoff and Thomas Mörs (NRM, Stockholm, Sweden), Benjamin Kear (PMU, Upssala, Sweden), Roula Pappa and Pip Brewer (NHMUK, London, United Kingdom), Patricia Holroyd (UCMP, Berkeley, USA), Samuel A. McLeod and Xiaoming Wang (NHMLA, Los Angeles, USA), Didier Berthet and François Vigouroux (Musée des confluences, Lyon, France), Béatrice Roussel (Musée de Valence, Valence, France), Loïc Costeur (NMBS, Basel, Switzerland), Susana Fraile and Jorge Morales (MNCN, Madrid, Spain), Daniel Brinkman and Vanessa R. Rhue (YPM, New Haven, USA), Jin Meng, Judith Galkin and Ruth O'Leary (AMNH, New York, USA) and finally Nicholas Pyenson, Amanda Millhouse and Matthew Miller (NMNH, Washington DC, USA).

For providing us additional scans, we would like to thank Denis Geraads, Florent Goussard, and Christine Argot (MNHN, Paris, France); Justin Adams (DNMNH, Pretoria, South Africa); Jeanette Pirlo and Sierra Steely (FLMNH, Gainesville, USA); Aly Baumgartner (FHSM, Hays, USA); Jamie A. MacLaren (UA, Antwerp, Belgium); Joan Madurell-Malapeira and David Alba (ICP, Sabadell, Spain); Xiaoming Wang (NHMLA, Los Angeles, USA); and Sina Dupuis (UZH, Zurich, Switzerland); see material list in ESM for details about scans that were shared. N.C. was supported by a grant from the Fonds de la Recherche Scientifique F.R.S.–FNRS (FRIA grant number FRIA FC 36251) and is currently supported by a Belgian American Educational Foundation (BAEF) post-doctoral fellowship. V.F. is supported by a grant from the Fonds de la Recherche Scientifique F.R.S.–FNRS (MIS F.4511.19). D.T. is grateful to NBFC, funded by the Italian Ministry of University and Research, PNRR, Missione 4 Componente 2, "Dalla ricerca all' impresa," Investimento 1.4, project CN00000033. D.T. also received support from "Avvio alla Ricerca 2019, 2020, and 2022" funding, which is financed by the University of Rome "La Sapienza." D.T. also received support from the SYNTHESYS Access Program that is financed by the European Community Research Infrastructure Action under the FP7 (ES-TAF-2750 awarded to D.T.).

N.C. would like to thank members of her Ph.D. committee (Bruno Frederich and Jamie MacLaren) and jury (Anne Claire Fabre, Carlo Meloro, and Jack Tseng) for their comments and discussion about this chapter.

AUTHOR CONTRIBUTIONS

Conceptualization, N.C., M.M., D.T., and V.F.; formal analysis, N.C.; investigation, N.C., M.M., D.T., and V.F.; methodology, N.C.; data acquisition, N.C., M.M., and D.T.; writing – review & editing, N.C., M.M., D.T., and V.F.

DECLARATION OF INTERESTS

The authors declare no competing interests.

Received: December 21, 2023
Revised: March 10, 2024
Accepted: April 24, 2024
Published: May 16, 2024

REFERENCES

1. Turner, A., and Antón, M. (1997). The Big Cats and Their Fossil Relatives: an Illustrated Guide to Their Evolution and Natural History (Columbia University Press).
2. McGhee, G.R. (2006). The Geometry of Evolution: Adaptive Landscapes and Theoretical Morphospaces (Cambridge University Press).
3. Van Valkenburgh, B. (2007). Deja vu: the evolution of feeding morphologies in the Carnivora. Integr. Comp. Biol. *47*, 147–163. https://doi.org/10.1093/icb/icm016.
4. Anton, M. (2013). Sabertooth, J.O. Farlow, ed. (Indiana University Press).
5. Turner, A., Antón, M., Salesa, M.J., and Morales, J. (2011). Changing ideas about the evolution and functional morphology of Machairodontine felids. Estud. Geol. *67*, 255–276. https://doi.org/10.3989/egeol.40590.188.
6. Emerson, S.B., and Radinsky, L. (1980). Functional analysis of sabertooth cranial morphology. Paleobiology *6*, 295–312. https://doi.org/10.1017/S0094837300006813.
7. Van Valkenburgh, B., and Jenkins, I. (2002). Evolutionary Patterns in the History of Permo-Triassic and Cenozoic Synapsid Predators. Paleontol. Soc. Pap. *8*, 267–288. https://doi.org/10.1017/S1089332600001121.
8. Martin, L.D., Babiarz, J.P., Naples, V.L., and Hearst, J. (2000). Three ways to be a saber-toothed cat. Naturwissenschaften *87*, 41–44. https://doi.org/10.1007/s001140050007.
9. Akersten, W.A. (1985). Canine function in Smilodon (Mammalia; Felidae; Machairodontinae). Contrib. Sci. *356*, 1–22. https://doi.org/10.5962/p.226830.
10. Antón, M., Galobart, A., and Turner, A. (2005). Co-existence of scimitar-toothed cats, lions and hominins in the European Pleistocene. Implications of the post-cranial anatomy of *Homotherium latidens* (Owen) for comparative palaeoecology. Quat. Sci. Rev. *24*, 1287–1301. https://doi.org/10.1016/J.QUASCIREV.2004.09.008.
11. Antón, M., Siliceo, G., Pastor, J.F., Morales, J., and Salesa, M.J. (2020). The early evolution of the sabre-toothed felid killing bite: the significance of the cervical morphology of *Machairodus aphanistus* (Carnivora: Felidae: Machairodontinae). Zool. J. Linn. Soc. *188*, 319–342. https://doi.org/10.1093/zoolinnean/zlz086.
12. Meachen-Samuels, J., and Van Valkenburgh, B. (2009). Forelimb indicators of prey-size preference in the felidae. J. Morphol. *270*, 729–744. https://doi.org/10.1002/jmor.10712.
13. Lautenschlager, S., Figueirido, B., Cashmore, D.D., Bendel, E.M., and Stubbs, T.L. (2020). Morphological convergence obscures functional diversity in sabre-toothed carnivores. Proc. Biol. Sci. *287*, 20201818. https://doi.org/10.1098/rspb.2020.1818.
14. Chatar, N., Fischer, V., and Tseng, Z.J. (2022). Many-to-one function of cat-like mandibles highlights a continuum of sabre-tooth adaptations. Proc. Biol. Sci. *289*, 20221627. https://doi.org/10.1098/rspb.2022.1627.
15. Slater, G.J., and Van Valkenburgh, B. (2008). Long in the tooth: evolution of sabertooth cat cranial shape. Paleobiology *34*, 403–419. https://doi.org/10.1666/07061.1.
16. Figueirido, B., Lautenschlager, S., Pérez-Ramos, A., and Van Valkenburgh, B. (2018). Distinct Predatory Behaviors in Scimitar- and Dirk-Toothed Sabertooth Cats. Curr. Biol. *28*, 3260–3266.e3. https://doi.org/10.1016/j.cub.2018.08.012.
17. Andersson, K., Norman, D., and Werdelin, L. (2011). Sabretoothed Carnivores and the Killing of Large Prey. PLoS One *6*, e24971. https://doi.org/10.1371/journal.pone.0024971.
18. Werdelin, L., Yamaguchi, N., Johnson, E., and Brien, S.J.O. (2010). Phylogeny and evolution of cats (Felidae). In Biology and Conservation of Wild Felids, D. Macdonald, and A. Loveridge, eds. (Oxford University Press), pp. 59–82.
19. Sakamoto, M., and Ruta, M. (2012). Convergence and Divergence in the Evolution of Cat Skulls: Temporal and Spatial Patterns of Morphological Diversity. PLoS One *7*, e39752. https://doi.org/10.1371/journal.pone.0039752.
20. Piras, P., Maiorino, L., Teresi, L., Meloro, C., Lucci, F., Kotsakis, T., and Raia, P. (2013). Bite of the cats: Relationships between functional integration and mechanical performance as revealed by mandible geometry. Syst. Biol. *62*, 878–900. https://doi.org/10.1093/sysbio/syt053.
21. Piras, P., Silvestro, D., Carotenuto, F., Castiglione, S., Kotsakis, A., Maiorino, L., Melchionna, M., Mondanaro, A., Sansalone, G., Serio, C., et al. (2018). Evolution of the sabertooth mandible: A deadly ecomorphological specialization. Palaeogeogr. Palaeoclimatol. Palaeoecol. *496*, 166–174. https://doi.org/10.1016/j.palaeo.2018.01.034.
22. Romano, M. (2019). Cranial disparity versus diversity in sabertoothed felids: A case of late morphospace saturation. J. Mediterr. Earth Sci. *11*, 81–92. https://doi.org/10.3304/JMES.2019.006.
23. Christiansen, P. (2008). Evolution of skull and mandible shape in cats (Carnivora: Felidae). PLoS One *3*, e2807. https://doi.org/10.1371/journal.pone.0002807.
24. Stayton, C.T. (2015). What does convergent evolution mean? The interpretation of convergence and its implications in the search for limits to evolution. Interface Focus *5*, 20150039. https://doi.org/10.1098/RSFS.2015.0039.
25. Castiglione, S., Serio, C., Tamagnini, D., Melchionna, M., Mondanaro, A., Di Febbraro, M., Profico, A., Piras, P., Barattolo, F., and Raia, P. (2019). A new, fast method to search for morphological convergence with shape data. PLoS One *14*, e0226949. https://doi.org/10.1371/JOURNAL.PONE.0226949.
26. Goswami, A., Watanabe, A., Felice, R.N., Bardua, C., Fabre, A.C., and Polly, P.D. (2019). High-Density Morphometric Analysis of Shape and Integration: The Good, the Bad, and the Not-Really-a-Problem. Integr. Comp. Biol. *59*, 669–683. https://doi.org/10.1093/icb/icz120.
27. Watanabe, A., Fabre, A.C., Felice, R.N., Maisano, J.A., Müller, J., Herrel, A., and Goswami, A. (2019). Ecomorphological diversification in squamates from conserved pattern of cranial integration. Proc. Natl. Acad. Sci. USA *116*, 14688–14697. https://doi.org/10.1073/pnas.1820967116.
28. Cheverud, J.M. (1982). Phenotypic, Genetic, and Environmental Morphological Integration in the Cranium. Evolution *36*, 499–516. https://doi.org/10.1111/j.1558-5646.1982.tb05070.x.
29. Hallgrímsson, B., Willmore, K., Dorval, C., and Cooper, D.M.L. (2004). Craniofacial variability and modularity in macaques and mice. J. Exp. Zool. B Mol. Dev. Evol. *302*, 207–225. https://doi.org/10.1002/jez.b.21002.
30. Wagner, G.P. (1996). Homologues, Natural Kinds and the Evolution of Modularity. Am. Zool. *36*, 36–43. https://doi.org/10.1093/icb/36.1.36.
31. Goswami, A., and Polly, P.D. (2010). Methods For studylng MorPhologlcal Integratlon and Modularlty. Paleontol. Soc. Pap. *16*, 213–243. https://doi.org/10.1017/S1089332600001881.
32. Klingenberg, C.P. (2010). Evolution and development of shape: integrating quantitative approaches. Nat. Rev. Genet. *11*, 623–635. https://doi.org/10.1038/nrg2829.
33. Klingenberg, C.P. (2008). Morphological Integration and Developmental Modularity. Annu. Rev. Ecol. Evol. Syst. *39*, 115–132. https://doi.org/10.1146/annurev.ecolsys.37.091305.110054.
34. Felice, R.N., Randau, M., and Goswami, A. (2018). A fly in a tube: Macroevolutionary expectations for integrated phenotypes. Evolution *72*, 2580–2594. https://doi.org/10.1111/EVO.13608.

35. Christiansen, P. (2006). Sabertooth characters in the clouded leopard (*Neofelis nebulosa* Griffiths 1821). J. Morphol. *267*, 1186–1198. https://doi.org/10.1002/jmor.10468.

36. Christiansen, P. (2008). Evolutionary convergence of primitive sabertooth craniomandibular morphology: the clouded leopard (*Neofelis nebulosa*) and *Paramachairodus ogygia* compared. J. Mammal. Evol. *15*, 155–179. https://doi.org/10.1007/s10914-007-9069-z.

37. Harano, T., and Kutsukake, N. (2018). Directional selection in the evolution of elongated upper canines in clouded leopards and sabre-toothed cats. J. Evol. Biol. *31*, 1268–1283. https://doi.org/10.1111/jeb.13309.

38. Seidensticker, J. (1976). On the Ecological Separation between Tigers and Leopards. Biotropica *8*, 225–234. https://doi.org/10.2307/2989714.

39. Bailey, T.N. (1993). The African Leopard: Ecology and Behavior of a Solitary Felid (Columbia University Press).

40. Law, C.J., Blackwell, E.A., Curtis, A.A., Dickinson, E., Hartstone-Rose, A., and Santana, S.E. (2022). Decoupled evolution of the cranium and mandible in carnivoran mammals. Evolution *76*, 2959–2974. https://doi.org/10.1111/EVO.14578.

41. Welsh, E., Boyd, C.A., and Spearing, K. (2020). Split carinae on a specimen of false saber-toothed cat (Carnivora: Nimravidae) and the implications for analogous tooth abnormality formation in mammals and theropod dinorsaurs. Proc. S. Dak. Acad. Sci. *99*, 69–82.

42. Cope, E.D. (1880). On the extinct cats of America. Am. Nat. *14*, 833–858. https://doi.org/10.1086/272672.

43. Welsh, E., Boyad, C.A., Spearing, K., and Barrett, P.Z. (2015). Stratigraphic and taxonomic revision of a north american false saber-toothed cat cub. Proc. S. Dak. Acad. Sci. *94*, 141–153.

44. Anton, M., Salesa, M.J., Morales, J., and Turner, A. (2004). First known complete skulls of the scimitar-toothed cat *Machairodus aphanistus* (Felidae, Carnivora) from the Spanish late Miocene site of Batallones-1. J. Vertebr. Paleontol. *24*, 957–969. https://doi.org/10.1671/0272-4634(2004)024[0957:FKCSOT]2.0.CO;2.

45. Antón, M., and Galobart, À. (1999). Neck function and predatory behavior in the scimitar toothed cat *Homotherium latidens* (Owen). J. Vertebr. Paleontol. *19*, 771–784. https://doi.org/10.1080/02724634.1999.10011190.

46. Meachen-Samuels, J.A., and van Valkenburgh, B. (2010). Radiographs Reveal Exceptional Forelimb Strength in the Sabertooth Cat, *Smilodon fatalis*. PLoS One *5*, e11412. https://doi.org/10.1371/JOURNAL.PONE.0011412.

47. Chatar, N., Fischer, V., Siliceo, G., Antón, M., Morales, J., and Salesa, M.J. (2021). Morphometric Analysis of the Mandible of Primitive Sabertoothed Felids from the late Miocene of Spain. J. Mammal. Evol. *28*, 753–771. https://doi.org/10.1007/s10914-021-09541-0.

48. Salesa, M.J., Antón, M., Turner, A., and Morales, J. (2006). Inferred behaviour and ecology of the primitive sabre-toothed cat *Paramachairodus ogygia* (Felidae, Machairodontinae) from the Late Miocene of Spain. J. Zool. *268*, 243–254. https://doi.org/10.1111/j.1469-7998.2005.00032.x.

49. Li, Y., and Spassov, N. (2017). A new species of *Paramachaerodus* (Mammalia, Carnivora, Felidae) from the late Miocene of China and Bulgaria, and revision of *Promegantereon* Kretzoi, 1938 and *Paramachaerodus* Pilgrim, 1913. PalZ *91*, 409–426. https://doi.org/10.1007/s12542-017-0371-7.

50. Monescillo, M.F.G., Salesa, M.J., Antón, M., Siliceo, G., and Morales, J. (2014). *Machairodus aphanistus* (Felidae, Machairodontinae, Homotherini) from the late Miocene (Vallesian, MN 10) site of Batallones-3 (Torrejón de Velasco, Madrid, Spain). J. Vertebr. Paleontol. *34*, 699–709. https://doi.org/10.1080/02724634.2013.804415.

51. Salesa, M.J., Antón, M., Turner, A., and Morales, J. (2005). Aspects of the functional morphology in the cranial and cervical skeleton of the sabre-toothed cat *Paramachairodus ogygia* (Kaup, 1832) (Felidae, Machairodontinae) from the Late Miocene of Spain: Implications for the origins of the machairodont killing bite. Zool. J. Linn. Soc. *144*, 363–377. https://doi.org/10.1111/j.1096-3642.2005.00174.x.

52. Averianov, A., Obraztsova, E., Danilov, I., Skutschas, P., and Jin, J. (2016). First nimravid skull from Asia. Sci. Rep. *6*, 25812. https://doi.org/10.1038/srep25812.

53. Peigné, S. (2001). A primitive nimravine skull from the Quercy fissures, France: implications for the origin and evolution of Nimravidae (Carnivora). Zool. J. Linn. Soc. *132*, 401–410. https://doi.org/10.1111/j.1096-3642.2001.tb02467.x.

54. Bryant, H.N. (1991). Phylogenetic Relationships and Systematics of the Nimravidae (Carnivora). J. Mammal. *72*, 56–78. https://doi.org/10.2307/1381980.

55. Melchionna, M., Profico, A., Castiglione, S., Serio, C., Mondanaro, A., Modafferi, M., Tamagnini, D., Maiorano, L., Raia, P., Witmer, L.M., et al. (2021). A method for mapping morphological convergence on three-dimensional digital models: the case of the mammalian sabre-tooth. Palaeontology *64*, 573–584. https://doi.org/10.1111/pala.12542.

56. Dayan, T., Simberloff, D., Tchernov, E., and Yom-Tov, Y. (1990). Feline Canines: Community-Wide Character Displacement Among the Small Cats of Israel. Am. Nat. *136*, 39–60. https://doi.org/10.1086/285081.

57. Peigné, S. (1999). *Proailurus*, l'un des plus anciens Felidae (Carnivora) d'Eurasie: systématique et évolution. Bull. Soc. Hist. Nat. Toulouse *135*, 125–134.

58. de Beaumont, G. (1961). Recherches sur *Felis attica* Wagner du Pontien eurasiatique avec quelques observations sur les genres *Pseudaelurus* Gervais et *Proailurus* Filhol. Nouvelles archives du Muséum d'histoire naturelle de Lyon *6*, 1X–45.

59. Sunquist, M., and Sunquist, F. (2002). Wild Cats of the World (University of Chicago Press).

60. Peterhans, J.C.K., Wrangham, R.W., Carter, M.L., and Hauser, M.D. (1993). A contribution to tropical rain forest taphonomy: retrieval and documentation of chimpanzee remains from Kibale Forest, Uganda. J. Hum. Evol. *25*, 485–514. https://doi.org/10.1006/jhev.1993.1063.

61. Behrensmeyer, A.K., Western, D., and Boaz, D.E.D. (1979). New Perspectives in Vertebrate Paleoecology from a Recent Bone Assemblage. Paleobiology *5*, 12–21. https://doi.org/10.1017/S0094837300006254.

62. Turner, A., and Antón, M. (1998). Climate and evolution: implications of some extinction patterns in African and European Machairodontine Cats of the Plio-Pleistocene. Estudios Geológicos *54*, 209–230.

63. Christiansen, P. (2012). Phylogeny of the sabertoothed felids (Carnivora: Felidae: Machairodontinae). Cladistics *29*, 543–559.

64. Stuart, A.J. (2015). Late Quaternary megafaunal extinctions on the continents: a short review. Geol. J. *50*, 338–363. https://doi.org/10.1002/GJ.2633.

65. Hetherington, A.J., Sherratt, E., Ruta, M., Wilkinson, M., Deline, B., and Donoghue, P.C.J. (2015). Do cladistic and morphometric data capture common patterns of morphological disparity? Palaeontology *58*, 393–399. https://doi.org/10.1111/pala.12159.

66. Wills, M.A., Briggs, D.E.G., and Fortey, R.A. (1994). Disparity as an Evolutionary Index: A Comparison of Cambrian and Recent Arthropods. Paleobiology *20*, 93–130. https://doi.org/10.1017/S009483730001263X.

67. Schaeffer, J., Benton, M.J., Rayfield, E.J., and Stubbs, T.L. (2020). Morphological disparity in theropod jaws: comparing discrete characters and geometric morphometrics. Palaeontology *63*, 283–299. https://doi.org/10.1111/pala.12455.

68. Hughes, M., Gerber, S., and Wills, M.A. (2013). Clades reach highest morphological disparity early in their evolution. Proc. Natl. Acad. Sci. USA *110*, 13875–13879. https://doi.org/10.1073/pnas.1302642110.

69. Schlager, S., Profico, A., Di Vincenzo, F., and Manzi, G. (2018). Retrodeformation of fossil specimens based on 3D bilateral semi-landmarks: Implementation in the R package "Morpho". https://doi.org/10.1371/journal.pone.0194073.

70. Meloro, C., and Slater, G.J. (2012). Covariation in the Skull Modules of Cats: The challenge of growing saber-like canines. J. Vertebr. Paleontol. *32*, 677–685. https://doi.org/10.1080/02724634.2012.649328.

71. Tamagnini, D., Michaud, M., Meloro, C., Raia, P., Soibelzon, L., Tambusso, P.S., Varela, L., and Maiorano, L. (2023). Conical and sabertoothed cats as an exception to craniofacial evolutionary allometry. Sci. Rep. *13*, 13571. https://doi.org/10.1038/s41598-023-40677-6.

72. R Core Team (2021). R: A Language and Environment for Statistical Computing (R Foundation for Statistical Computing).

73. AMETEK Inc (2023). VXmodel. https://www.creaform3d.com/en.

74. Blender Online Community (2023). Blender - a 3D modelling and rendering package (Blender Institute). https://manpages.ubuntu.com/manpages/xenial/en/man1/blender.1.html.

75. Cigoni, P., Callieri, M., and Corsini, M. (2008). Meshlab: an open-source mesh processing tool. ERCIM NEWS *73*, 47–48.

76. Schlager, S. (2017). Morpho and Rvcg – Shape Analysis in R: R-Packages for Geometric Morphometrics, Shape Analysis and Surface Manipulations. Stat. Shape Deform. Anal.: Methods Implement. Appl. 217–256. https://doi.org/10.1016/B978-0-12-810493-4.00011-0.

77. Robles, J.M., Alba, D.M., Fortuny, J., De Esteban-Trivigno, S.D., Rotgers, C., Balaguer, J., Carmona, R., Galindo, J., Almécija, S., Bertó, J.V., et al. (2013). New craniodental remains of the barbourofelid *Albanosmilus jourdani* (Filhol, 1883) from the Miocene of the Vallès-Penedès Basin (NE Iberian Peninsula) and the phylogeny of the Barbourofelini. J. Syst. Palaeontol. *11*, 993–1022. https://doi.org/10.1080/14772019.2012.724090.

78. Tseng, Z.J., Wang, X., Slater, G.J., Takeuchi, G.T., Li, Q., Liu, J., and Xie, G. (2014). Himalayan fossils of the oldest known pantherine establish ancient origin of big cats. Proc. Biol. Sci. *281*, 20132686. https://doi.org/10.1098/rspb.2013.2686.

79. Spassov, N., and Geraads, D. (2015). A New Felid from the Late Miocene of the Balkans and the Contents of the Genus *Metailurus* Zdansky, 1924 (Carnivora, Felidae). J. Mammal. Evol. *22*, 45–56. https://doi.org/10.1007/s10914-014-9266-5.

80. Adams, J.W., Olah, A., McCurry, M.R., and Potze, S. (2015). Surface Model and Tomographic Archive of Fossil Primate and Other Mammal Holotype and Paratype Specimens of the Ditsong National Museum of Natural History, Pretoria, South Africa. PLoS One *10*, e0139800. https://doi.org/10.1371/journal.pone.0139800.

81. Geraads, D., and Spassov, N. (2020). A skull of *Machairodus* Kaup, 1833 (Felidae, Mammalia) from the late Miocene of Hadjidimovo (Bulgaria), and its place in the evolution of the genus. Geodiversitas *42*, 123–137. https://doi.org/10.5252/geodiversitas2020v42a9.

82. Wang, X., White, S.C., and Guan, J. (2020). A new genus and species of sabretooth, *Oriensmilus liupanensis* (Barbourofelinae, Nimravidae, Carnivora), from the middle Miocene of China suggests barbourofelines are nimravids, not felids. J. Syst. Palaeontol. *18*, 783–803. https://doi.org/10.1080/14772019.2019.1691066.

83. Bookstein, F. (1991). Morphometric Tools for Landmark Data: Geometry and Biology (Camridge University Press).

84. Stratovan Corporation. Stratovan Checkpoint. Preprint. https://www.stratovan.com/products/checkpoint.

85. Adams, D.C., and Otárola-Castillo, E. (2013). geomorph: an r package for the collection and analysis of geometric morphometric shape data. Methods Ecol. Evol. *4*, 393–399. https://doi.org/10.1111/2041-210X.12035.

86. Barrett, P.Z. (2021). The largest hoplophonine and a complex new hypothesis of nimravid evolution. Sci. Rep. *11*, 21078. https://doi.org/10.1038/s41598-021-00521-1.

87. Jiangzuo, Q., Werdelin, L., and Sun, Y. (2022). A dwarf sabertooth cat (Felidae: Machairodontinae) from Shanxi, China, and the phylogeny of the sabertooth tribe Machairodontini. Quat. Sci. Rev. *284*, 107517. https://doi.org/10.1016/j.quascirev.2022.107517.

88. Slater, G.J., and Friscia, A.R. (2019). Hierarchy in adaptive radiation: A case study using the Carnivora (Mammalia). Evolution *73*, 524–539. https://doi.org/10.1111/evo.13689.

89. Paradis, E., and Schliep, K. (2019). Ape 5.0: An environment for modern phylogenetics and evolutionary analyses in R. Bioinformatics *35*, 526–528. https://doi.org/10.1093/bioinformatics/bty633.

90. Chatar, N., Michaud, M., and Fischer, V. (2022). Not a jaguar after all? Phylogenetic affinities and morphology of the Pleistocene felid *Panthera gombaszoegensis*. Pap. Palaeontol. *8*, e1464. https://doi.org/10.1002/spp2.1464.

91. Rothwell, T. (2003). Phylogenetic systematics of North American *Pseudaelurus* (Carnivora: Felidae). Am. Mus. Novit. *3403*, 1–64. https://doi.org/10.1206/0003-0082(2003)403<0001:PSONAP>2.0.CO;2.

92. Collier, G.E., and O'Brien, S.J. (1985). A molecular phylogeny of the Felidae: immunological distance. Evolution *39*, 473–487. https://doi.org/10.1111/J.1558-5646.1985.TB00389.X.

93. Johnson, W.E., Eizirik, E., Pecon-Slattery, J., Murphy, W.J., Antunes, A., Teeling, E., and O'Brien, S.J. (2006). The late miocene radiation of modern felidae: A genetic assessment. Science *311*, 73–77. https://doi.org/10.1126/science.1122277.

94. Figueiró, H.V., Li, G., Trindade, F.J., Assis, J., Pais, F., Fernandes, G., Santos, S.H.D., Hughes, G.M., Komissarov, A., Antunes, A., et al. (2017). Genome-wide signatures of complex introgression and adaptive evolution in the big cats. Sci. Adv. *3*, e1700299. https://doi.org/10.1126/sciadv.1700299.

95. Bapst, D.W. (2012). paleotree: an R package for paleontological and phylogenetic analyses of evolution. Methods Ecol. Evol. *3*, 803–807. https://doi.org/10.1111/j.2041-210X.2012.00223.x.

96. Barrett, P.Z., Hopkins, S.S.B., and Price, S.A. (2021). How many sabertooths? Reevaluating the number of carnivoran sabretooth lineages with total-evidence Bayesian techniques and a novel origin of the Miocene Nimravidae. J. Vertebr. Paleontol. *41*, 1–15. https://doi.org/10.1080/02724634.2021.1923523.

97. Sakamoto, M., Lloyd, G.T., and Benton, M.J. (2010). Phylogenetically structured variance in felid bite force: the role of phylogeny in the evolution of biting performance. J. Evol. Biol. *23*, 463–478. https://doi.org/10.1111/j.1420-9101.2009.01922.x.

98. Madurell-Malapeira, J., Rodríguez-Hidalgo, A., Aouraghe, H., Haddoumi, H., Lucenti, S.B., Oujaa, A., Saladié, P., Bengamra, S., Marín, J., Souhir, M., et al. (2021). First small-sized *Dinofelis*: Evidence from the Plio-Pleistocene of North Africa. Quat. Sci. Rev. *265*, 107028. https://doi.org/10.1016/J.QUASCIREV.2021.107028.

99. Fischer, V., MacLaren, J.A., Soul, L.C., Bennion, R.F., Druckenmiller, P.S., and Benson, R.B.J. (2020). The macroevolutionary landscape of short-necked plesiosaurians. Sci. Rep. *10*, 16434. https://doi.org/10.1038/s41598-020-73413-5.

100. Christiansen, P., and Adolfssen, J.S. (2005). Bite forces, canine strength and skull allometry in carnivores (Mammalia, Carnivora). J. Zool. *266*, 133–151. https://doi.org/10.1017/S0952836905006643.

101. Slater, G.J., and Van Valkenburgh, B. (2009). Allometry and performance: The evolution of skull form and function in felids. J. Evol. Biol. *22*, 2278–2287. https://doi.org/10.1111/j.1420-9101.2009.01845.x.

102. Tamagnini, D., Meloro, C., and Cardini, A. (2017). Anyone with a Long-Face? Craniofacial Evolutionary Allometry (CREA) in a Family of Short-Faced Mammals, the Felidae. Evol. Biol. *44*, 476–495. https://doi.org/10.1007/S11692-017-9421-Z.

103. Guillerme, T. (2018). dispRity: A modular R package for measuring disparity. Methods Ecol. Evol. *9*, 1755–1763. https://doi.org/10.1111/2041-210X.13022.

104. Brusatte, S.L., Butler, R.J., Prieto-Márquez, A., and Norell, M.A. (2012). Dinosaur morphological diversity and the end-Cretaceous extinction. Nat. Commun. *3*, 804. https://doi.org/10.1038/ncomms1815.

105. Butler, R.J., Brusatte, S.L., Andres, B., and Benson, R.B.J. (2012). How do geological sampling biases affect studies of morphological

evolution in deep time? A case study of pterosaur (Reptilia: Archosauria) disparity. Evolution *66*, 147–162. https://doi.org/10.1111/J.1558-5646.2011.01415.X.

106. Prentice, K.C., Ruta, M., and Benton, M.J. (2011). Evolution of morphological disparity in pterosaurs. J. Syst. Palaeontol. *9*, 337–353. https://doi.org/10.1080/14772019.2011.565081.

107. Harmon, L.J., Weir, J.T., Brock, C.D., Glor, R.E., and Challenger, W. (2008). GEIGER: investigating evolutionary radiations. Bioinformatics *24*, 129–131. https://doi.org/10.1093/BIOINFORMATICS/BTM538.

108. Grossnickle, D.M., Brightly, W.H., Weaver, L.N., Stanchak, K.E., Roston, R.A., Pevsner, S.K., Stayton, C.T., Roston, R.A., and Law, C.J. (2022). A cautionary note on quantitative measures of phenotypic convergence. BioRxiv. https://doi.org/10.1101/2022.10.18.512739.

109. Castiglione, S., Serio, C., Mondanaro, A., Melchionna, M., Carotenuto, F., Di Febbraro, M., Profico, A., Tamagnini, D., and Raia, P. (2020). Ancestral State Estimation with Phylogenetic Ridge Regression. Evol. Biol. *47*, 220–232. https://doi.org/10.1007/s11692-020-09505-x.

Please cite this article in press as: Chatar et al., Evolutionary patterns of cat-like carnivorans unveil drivers of the sabertooth morphology, Current Biology (2024), https://doi.org/10.1016/j.cub.2024.04.055

STAR★METHODS

KEY RESOURCES TABLE

REAGENT or RESOURCE	SOURCE	IDENTIFIER
Deposited data		
3D Surface scans	https://www.morphosource.org/projects/000548886?locale=en	See Data S1 for complete list with specimen numbers
Landmark coordinates	Online supplemental information + https://hdl.handle.net/2268/316060	Online supplemental information & Orbi.
Specimen list with metadata	Online supplemental information + https://hdl.handle.net/2268/316060	See Data S1 & Orbi.
Software and algorithm		
R Studio v 4.2.3	R Core Team[72]	https://www.r-project.org
VX Models	AMETEK, Inc.[73]	https://www.creaform3d.com/
Stratovan checkpoint v2018.08.07	Stratovan Corporation	https://www.stratovan.com/
Blender	Blender Foundation[74]	blender.org
Meshlab	ISTI – CNR[75]	http://www.meshlab.net/

RESOURCE AVAILABILITY

Lead contact

Further information and requests for resources and reagents should be directed to and will be fulfilled by the lead contact, Narimane Chatar (narimane.chatar@uliege.be).

Materials availability

3D models used to perform the analyses are available on (Project ID: 000548886, https://www.morphosource.org/projects/000548886). For scans not available on MorphoSource (for instance, material that is not yet described) please contact Narimane Chatar (narimane.chatar@uliege.be) or the corresponding museum curator.

Data and code availability

All original code is available on Orbi, the ULiège Open Repository (https://hdl.handle.net/2268/316060) and Github (https://github.com/cha-nar) and is publicly available as of the date of publication as well as all the data: Landmark coordinates, Excel files containing the full material list with metadata, sliding sequence for landmarks, measurements, FAD and LAD.

EXPERIMENTAL MODEL AND SUBJECT DETAILS

The dataset is composed of a total of 189 3D models, 99 mandibles (91 different taxa) and 90 crania (88 different taxa). Our dataset exclusively contains felids and nimravids: Respectively 32% and 37% of sampled mandibular and cranial specimens belong to living species (See Data S1A and S1D for detailed list of specimens including metadata), covering 33 out of the 42 (78%) recognized extant taxa. All specimens were adults and analyses were performed on the specimens themselves rather than species average.

Retrodeformation and missing data estimation

Some specimens were mirrored using VX models, as we chose to landmark only one side of each structure. Different repair tools were used to fix specimens that were slightly incomplete, this step was done in VX models and/or Blender. However, for some specimens lacking more consistent parts, we employed various reconstruction techniques. Figures showing specimens before and after retrodeformations are available on Orbi (https://hdl.handle.net/2268/316060).

Retrodeformation

Some fossil crania appeared relatively complete but underwent basic shearing induced by taphonomic processes. For those specimens, we retrodeformed them using the protocol described in Schlager et al.[69] To do so, we placed landmarks from our landmarking procedure that do not lie on the symmetry plane of the cranium (Landmarks 5, 6, 10, 11, 12, 13, 14,15, 16,17, 18, 20, 21 as well as curves 3, 4, 6, 7; see Figure S1). This procedure was performed using the Morpho package.[76] The specimens retrodeformed using this method were: *Panthera zdansky* (BC-294) *Dinofelis abeli* (AMNH-F-AM-50445) and *Panthera palaeosinensis* (PMU 21780-1) (See retrodeformations Figures on Orbi).

Please cite this article in press as: Chatar et al., Evolutionary patterns of cat-like carnivorans unveil drivers of the sabertooth morphology, Current Biology (2024), https://doi.org/10.1016/j.cub.2024.04.055

Other specimens underwent basic compression (along one axis). For those specimens, we used Blender to correct the deformations. Those specimens include *Eusmilus adelos* (USNM-12820), *Eusmilus sicarius* (YPM-VPPU-012953), *Metailurus* sp (AMNH-131854), *Metailurus_parvulus* (NHMUK-PV-OR-28862) and *Megantereon cultridens* (MNHN.F.PET2001a) (See retrodeformations Figures on Orbi).

Missing landmarks estimation

Some specimens were still too incomplete to landmark fully, so we used missing landmark estimation. The proportion of specimens exhibiting missing data was 8% for the mandibles (8/99) and 21% for the crania (19/90) (See orange lines in Data S1A and S1D). However, we still excluded specimens that were too incomplete and used missing data estimation only when a fragment of the bone was missing, for instance a fragment of coronoid process missing on a mandible (curve 1 and potentially landmark 1) or the zygomatic arches missing on a cranium (Landmarks 18, 6 and curve 3). This estimation was performed using the fixLMtps function of the Morpho package[76] that estimates missing landmarks by mapping weighted averages from complete datasets onto the missing specimen using the three closest observations.

METHOD DETAILS

Digitization

Novel scans realized for this study were obtained using a Creaform HandySCAN 300 laser surface scanner with a resolution varying from 0.2 mm to 0.5 mm (see supplemental information). Scans were initially cleaned, merged, and exported in ply format using VXElements v.6.0. Models were then treated using VXmodel. Additional models were obtained from (Robles et al.[77] (*Albanosmilus jourdani*); Tseng et al.[78] (*Panthera blytheae*); Spassov and Geraads[79] (*Yoshi garevskii*); Adams et al.[80] (*Dinofelis barlowi*, *Dinofelis piveteaui*) Geraads and Spassov[81] (*Amphimachairodus giganteus*); Wang et al.[82] (*Oriensmilus liupanensis*)) see Data S1 for details.

Morphometric data collection

We placed eleven type-II landmarks[83] and three curves composed of 27 semi-landmarks on the mandible (Figure S1; Data S1A) using Stratovan checkpoint v2018.08.07[84] and exporting the coordinates as '.pts' files. On the cranium, we placed a total of twenty-two type-II landmarks + type-III landmarks and seven curves composed of 50 semi-landmarks (Figure S1; Data S1D). All analyses were then performed in the R v 4.2.3 statistical environment.[72] See Tables S1 and S2 for the description of each landmark used. Landmark coordinates were imported into R using the custom function 'import.pts' (https://github.com/cha-nar/importpts). Stratovan checkpoint exports all the missing coordinates as '9999' missing values were replaced by 'NA' using imbricated loops to allow the fixLMtps function from the Morpho package[76] to estimate the missing coordinates using weighted averages from the three most morphologically similar, complete, configurations. which uses weighted averages.

Generalized Procrustes superimposition was performed using the gpagen function from the geomorph package v4.0.5[85] specifying the semi-landmarks to slide using the 'curve' argument (Data S1B and S1E). Log centroid size was extracted from cranial shape data during Procrustes superimposition and used as a proxy of overall size.

Phylogeny

To assess the influence of phylogeny in our results and visualization purposes, we built a composite tree containing extant carnivorans, nimravids, and machairodontine felids in R by binding the trees published by Barrett,[86] Jiangzuo et al.,[87] and Slater and Friscia[88] using the 'bind.tree' function of the ape package.[89]

We dropped the tips absent from our dataset using the 'drop.tip' function. In the machairodontine tree, we also removed *Panthera leo* and *Lynx rufus* as they were already present in the extant carnivoran tree and did the same for *Homotherium serum*, *Smilodon populator* in the extant carnivoran tree. Twenty nine taxa were absent from the sampled trees and had to be manually added in positions found in the literature: *Yoshi minor*, *Yoshi garevskii, Amphimachairodus palanderi, Nimravides pediomonus Nimravides thinobastes, Machairodus catacopis, Smilodon gracilis, Pseudaelurus stouti, Pseudaelurus intrepidus, Pseudaelurus marshi, Pseudaelurus skineri, Pseudaelurus pedionomus*, *Pseudaelurus validus*, *Acinonyx pardinensis, Catopuma temminckii, Felis sylvestris, Leopardus pajeros, Leopardus wideii, Leptailurus serval, Miracinonyx studeri, Miracinonyx inexpectatus, Panthera atrox, Panthera speleae, Panthera paleosinensis, Panthera gombaszoegensis*, *Puma yaguarondi*, *Panthera uncia*, and *Puma pardoides*.[87,90–94]

We time-scaled the resulting supertree using the 'timePaleoPhy' function from the Paleotree package[95] through the minimum branch length (mbl) method. Divergence between Felidae and Nimravidae was set based on the results published by Barrett et al.[96] We generated the time tree using the 'geoscalePhylo' function from the paleotree package[95] with first and last occurrence dates obtained from the literature[79,86,87,90,91,97,98] or from the PBDB (paleobiodb.org) (see Data S1C and S1F). The super tree is available in Newick format on Orbi (https://hdl.handle.net/2268/316060).

Spatiotemporal distribution

To understand the spatiotemporal distribution of cat-like carnivorans and assess the influence of environmental factors on the evolution of disparity and diversity through time, we collected time (epoch and age) and localization data (continent and

Please cite this article in press as: Chatar et al., Evolutionary patterns of cat-like carnivorans unveil drivers of the sabertooth morphology, Current Biology (2024), https://doi.org/10.1016/j.cub.2024.04.055

country or state) for all sampled species (Data S1A and S1D). We duplicated entries in the dataset only when a species is recorded in multiple time bins or multiple geographical bins. Due to its length compared to other Epoch, the Miocene was divided into two sub-Epoch for the disparity analyses as it might have affected our results. Early Miocene corresponding to Aquitanian, Burdigalian and Langhian (23.03 to 13.82 Ma) and Late Miocene corresponding to Serravallian, Tortonian and Messinian (13.82 to 5.333 Ma).

QUANTIFICATION AND STATISTICAL ANALYSIS

Craniomandibular shape variation

A principal components analysis (PCA) was performed using the gm.prcomp function of the geomorph package v4.0.5[85] to assess the primary aspects of shape variation and morphospace occupation. To visualise the areas of recuring morphologies (in the sense of frequently colonised) in our morphospace, we computed the kernel density of occupation by modifying the script from Fischer et al.[99] To better visualize shape changes in the morphospace we used the plot_3D_bt_shape custom function https://github.com/cha-nar/plot_3D_bt_morphospace) (see Figure S2) to create a 3D backtransform morphospace.

To ensure that the larger sample size of living cats does not disproportionately influence the variance of the eigenvectors, we implemented a loop to randomly exclude 20 out of the 33 extant felid species from our set of Procrustes coordinates for the mandibular dataset. This reduction brought the number of extant species to 13, a sample size comparable to that of our nimravines (N=12) and barbourofelines (N=9). Subsequently, we conducted a Principal Component Analysis (PCA) on this artificially reduced dataset (those morphospaces are available on Orbi https://hdl.handle.net/2268/316060). Notably, the predominant shape variation observed was attributed to fossil taxa, even when only a dozen extant species were included. We used the procD.lm function from the geomorph package v4.0.5 to test the influence of the size on shape (allometry) on our shape data as previous studies shown that allometry is pervasive in felids.[100–102] We used the physignal function from the geomorph package v4.0.5[85] to quantify the phylogenetic signal from Procrustes shape variables in both crania and mandibles within the whole dataset and per clades (See Table S4).

Disparity

We used the dispRity package v1.7.0[103] to compare clade disparities (Felinae, Machairodontinae, Nimravinae, and Barbourofelinae). Morphological disparity was estimated as a bootstrapped sum of variances (1000 bootstraps). Then we computed the global disparity through time in cat-like carnivorans as both a bootstrapped sum of ranges and a bootstrapped sum of variances (1000 bootstraps), for each time bin (Eocene, Oligocene, Miocene, Pliocene, Pleistocene, and Extant). Sum of variances captures the dispersal of taxa within morphospace and can be influenced with the intensity of sampling, while the sum of ranges indicates the amount of overall morphospace occupation and can be biased by extreme yet rare morphologies. Those two metrics are therefore commonly combined to yield an honest picture of disparity (e.g; Wills et al.,[66] Brusatte et al.,[104] Butler et al.,[105] and Prentice et al.[106]). For comparison, we also computed the phylogenetically informed disparity through time using the dtt function from the Geiger package[107] using 1000 simulations and with a 95% CI. See FigureS4.

Convergence

We assessed the significance of the evolutionary convergence pairs of taxa using the CalconvCt function from the convevol package v2.0.0 to extract C-metrics (Stayton[24]; Grossnickle et al., 2023[108]) as well as the method implemented by Castiglione et al.[25] in the RRPhylo package.[109] Convergence and conservatism are two evolutionary processes resulting in distantly related phylogenetic tips with similar morphology. While Stayton's traditional C-measures are significant only in presence of convergence, the theta by Castiglione et al.[25] can be significant with both convergence or conservatism. Using a combination of those metrics can therefore help us distinguish between the two evolutionary patterns: significant C1 and theta indicates convergence, non-significant C1 and significant theta stands for conservatism, and non-significant C1 and theta indicate the absence of both convergence and conservatism. Traditional C-measures became widely used as they can distinguish between convergence and conservatism, which both those process resulting in distantly related phylogenetic tips with similar morphology. However, those metrics are extremely slow to compute, and Castiglione's method considers the time spent since their cladogenetic divergence where the temporal is thus important. We applied both those on the whole set of Procrustes coordinates as the occurrence of spurious patterns of convergence can increase in reduced shape spaces. See Figures S2G and S2H for a graphical representation of the convergence pairs tested, only C1 results are shown in the main document (see Table 1), C2-C4 results are available in Table S3. See Figure S3 for tanglegrams showing the correspondences between the phylogenetic supertree and the hierarchical cluster build from the distance matrix based on the Procrustes coordinates.

Patterns of phenotypic integration

To assess the potential role of phenotypic integration in sabertooth disparity we investigated patterns of integration between different craniomandibular modules (seven combinations in total). To do so, we performed phylogenetic two-block partial least squares analyses (2B-PLS) using the phylo.integration function from the geomorph package[85] on the resiudals from shape on size as size-related shape differences could inflate integration results. We then use the pls coefficient (r-PLS) as an estimation of

the degree of phenotypic integration between the two structures. The significance of the r-PLS coefficient is evaluated using 1000 permutations against the hypothesis of a complete absence of covariation between blocks.

Rate of morphological evolution

We investigated branch-specific evolutionary rates of evolution through time in the craniomandibular complex using the RRphylo function from the RRPhylo package.[109]

Current Biology, Volume *34*

Supplemental Information

Evolutionary patterns of cat-like carnivorans unveil drivers of the sabertooth morphology

Narimane Chatar, Margot Michaud, Davide Tamagnini, and Valentin Fischer

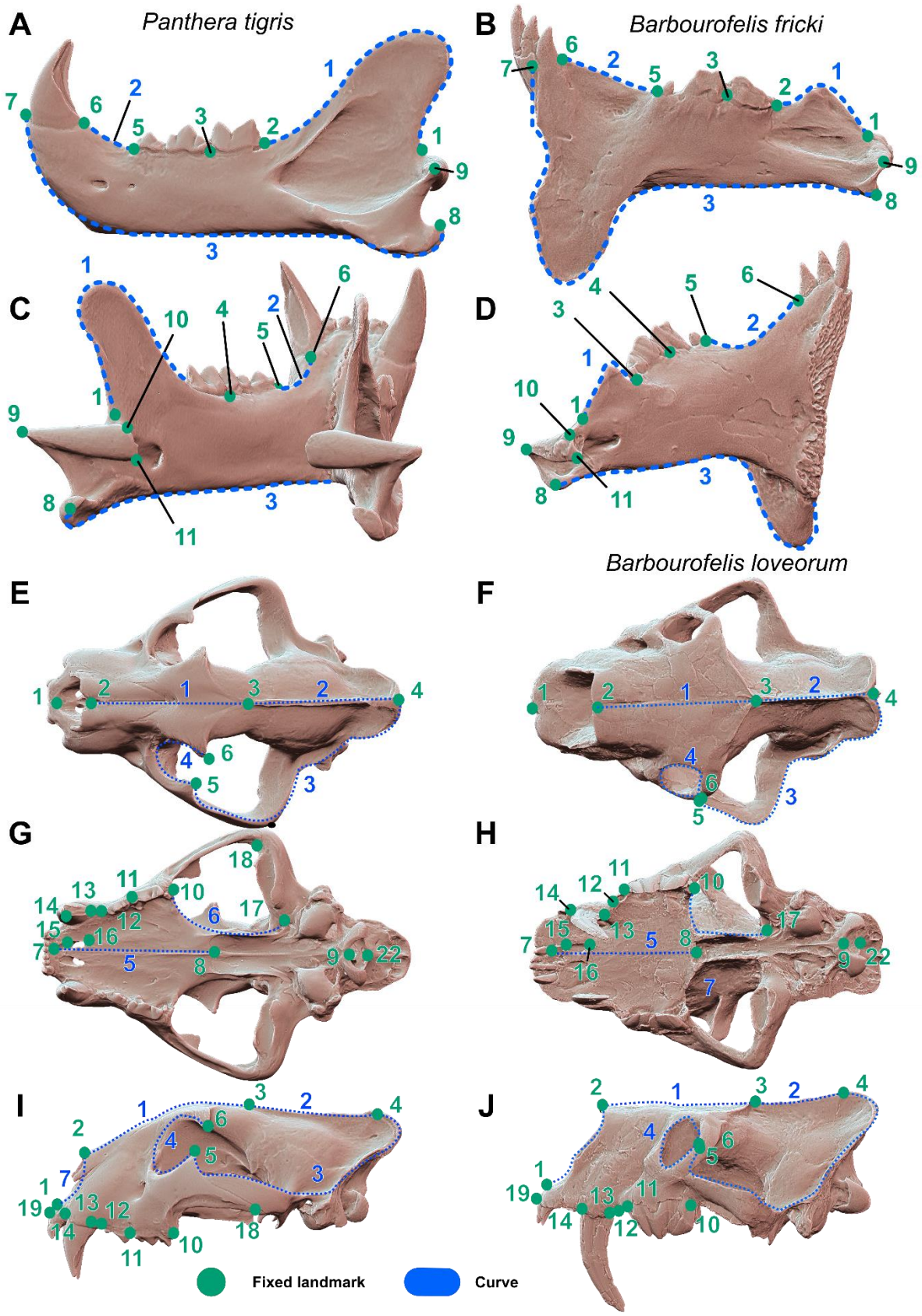

Figure S1: Landmark configuration used on the 99 mandibles with *Panthera tigris* (A, C) *and Barbourofelis fricki* (B, D) as examples. Related to STAR Methods, Table S1-S2. A-B: left lateral view; C-D: left anterolateral view; E-F: left posteromedial view. Landmark configuration used on the 90 crania with *Panthera tigris* (E, G, I) *and Barbourofelis loveorum* (F, H, J) as examples. E-F: dorsal view; G-H: ventral view; I-J: left lateral. .

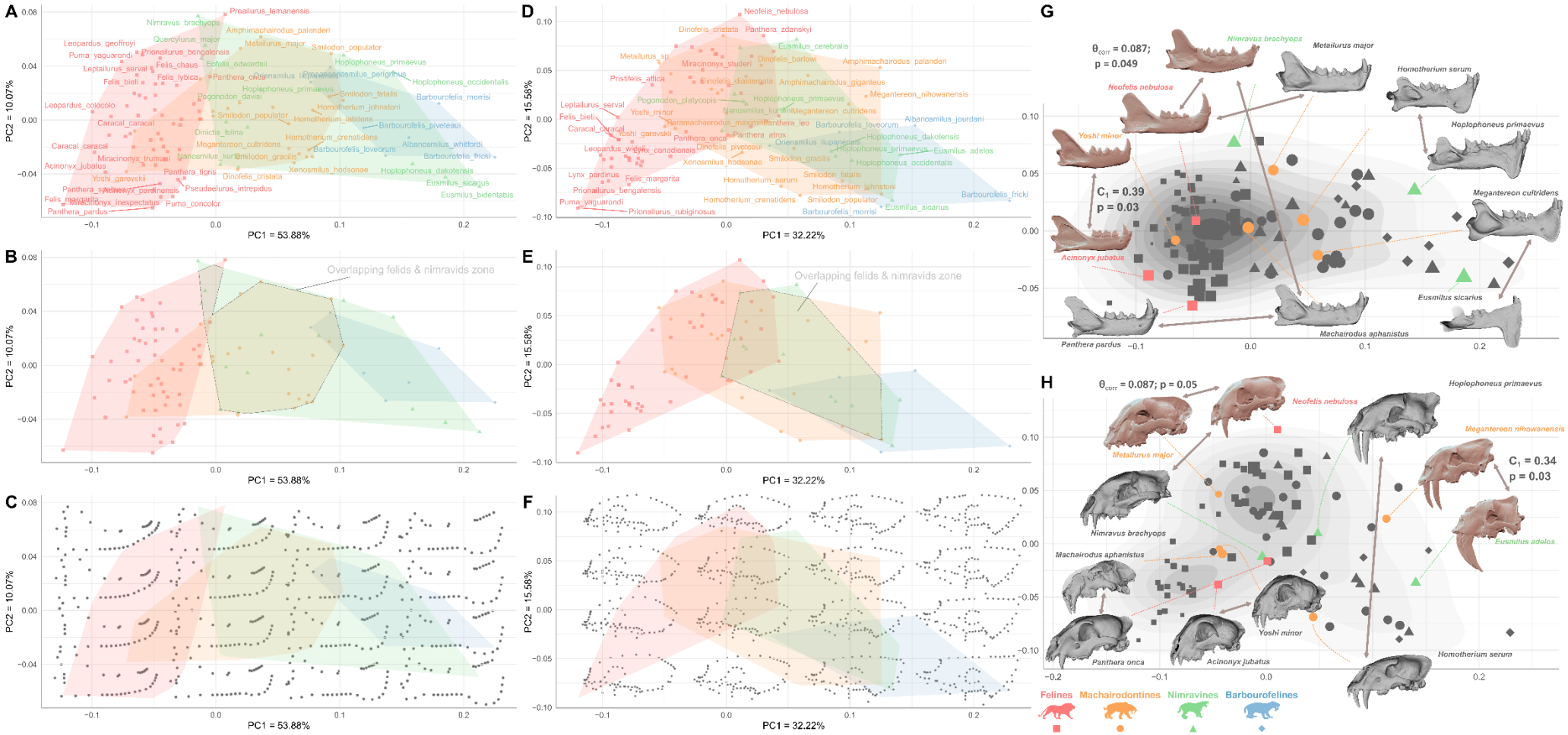

Figure S2: PCA on the mandible dataset showing A label of the species, B overlapping zone between felids and nimravids and C backtransfrom shapes in a grid pattern showing more intuitively how shape varies across morphospace. Related to Figure 1, Table 1, Table S3 and STAR Methods. PCA on the cranium dataset showing B label of the species, C overlapping zone between felids and nimravids and D backtransfrom shapes in a grid pattern showing more intuitively how shape varies across morphospace. Figure illustrating pairs that were found convergent following one of the two metrics used for G the mandible and H the cranium.

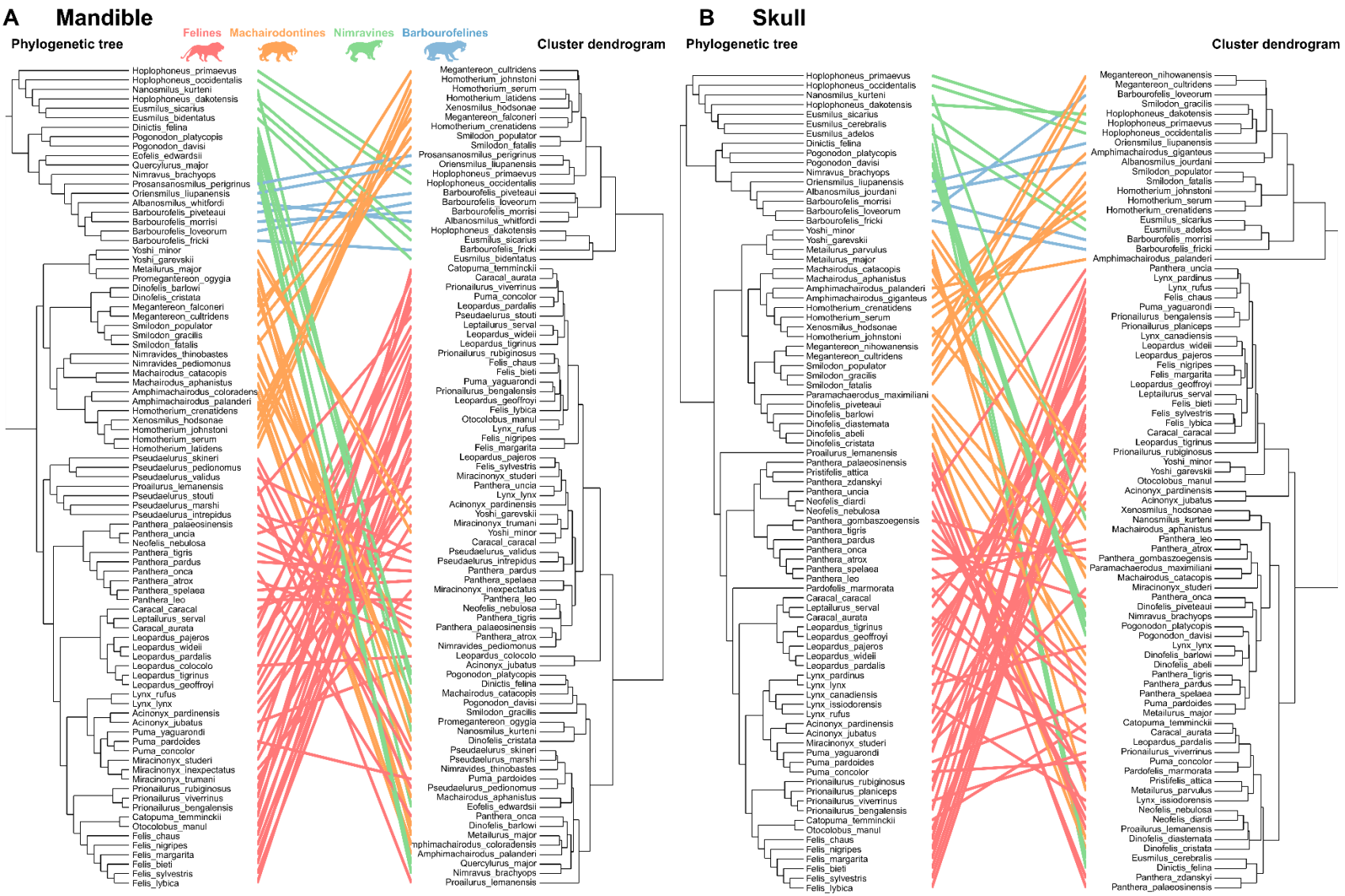

Figure S3: Tanglegram showing the correspondences between the phylogenetic supertree (left) and the hierarchical cluster build from the distance matrix based on the Procrustes coordinates (right) for the mandible dataset for A the mandible and B the cranium. Related to STAR Methods.

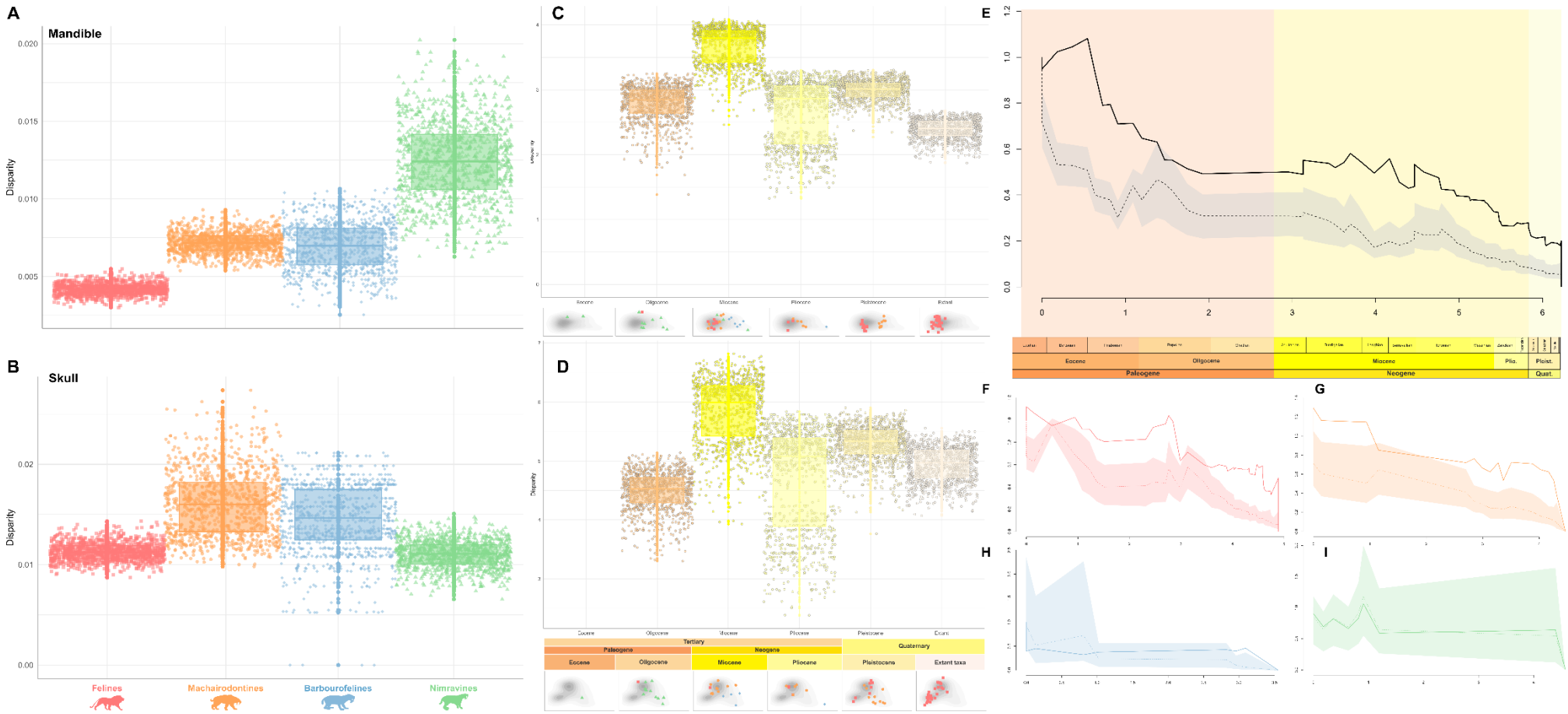

Figure S4: A-B Disparity per clade as A a sum of variances for the mandible and B the cranium (bottom). C-D Disparity trough time computed as C a sum of range in the cat like mandible with occupation of the morphospace at each Epoch and D as a sum of variance in the cat like cranium with occupation of the morphospace at each Epoch. E-I Disparity through time curves obtained through the dtt function. Related to Figure 2 and STAR methods. The dotted lines represent values of trait disparity expected under Brownian motion by simulating shape evolution 10000 times across the tree. Time values are relatives, 0.0 represents the root and 1.0 the tip of the phylogeny. Shaded areas indicate the 95% confidence interval for the simulations. E was produced on the whole dataset while F-I were produced for each group (F felinae s.l., G machirodontinae, H barbourofelinae and I nimravinae; each time axis being therefore relative to the root and tip of each of those groups).

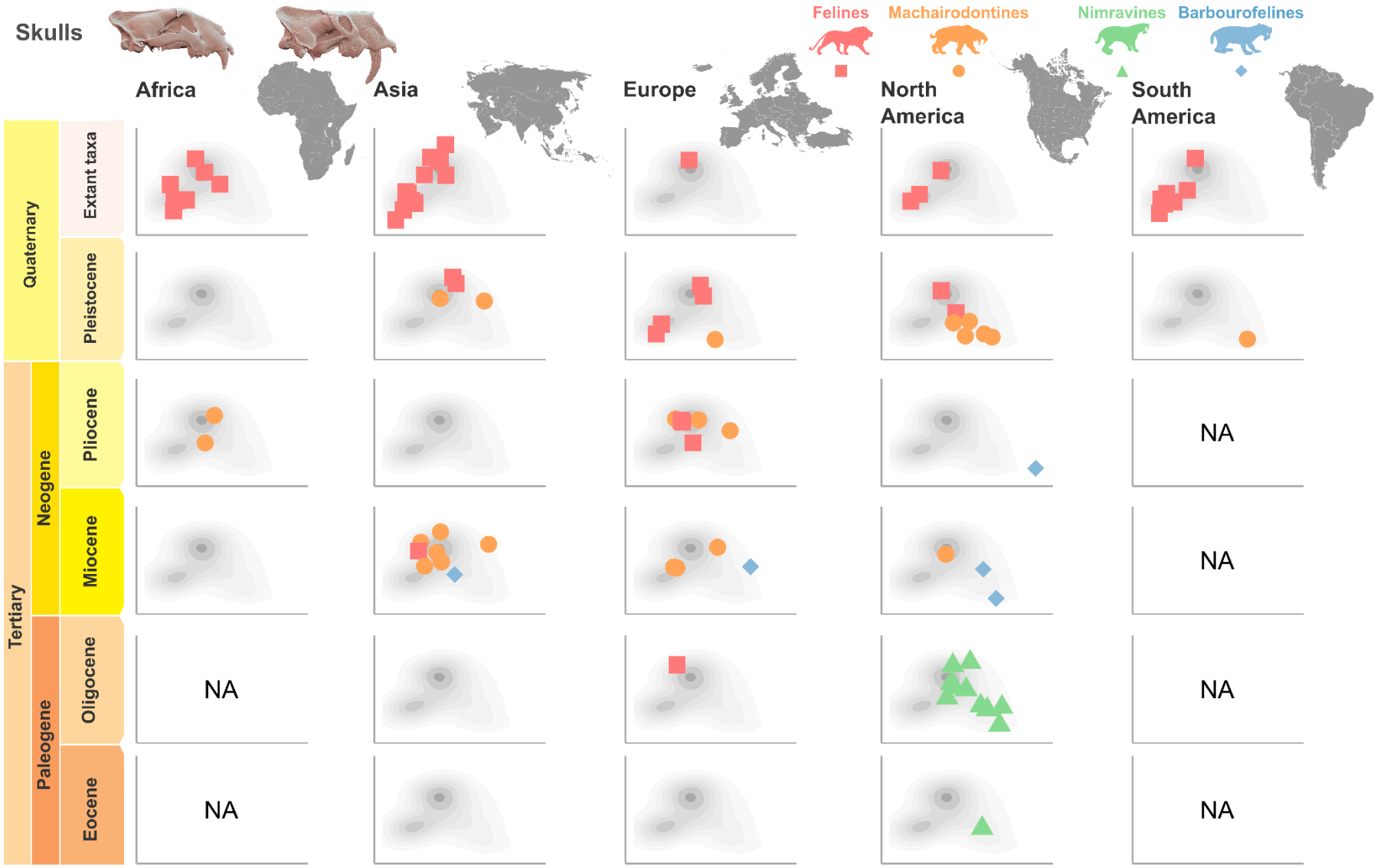

Figure S5: Occupation of the morphospace trough time and space for the skull data. Related to Figure 3.

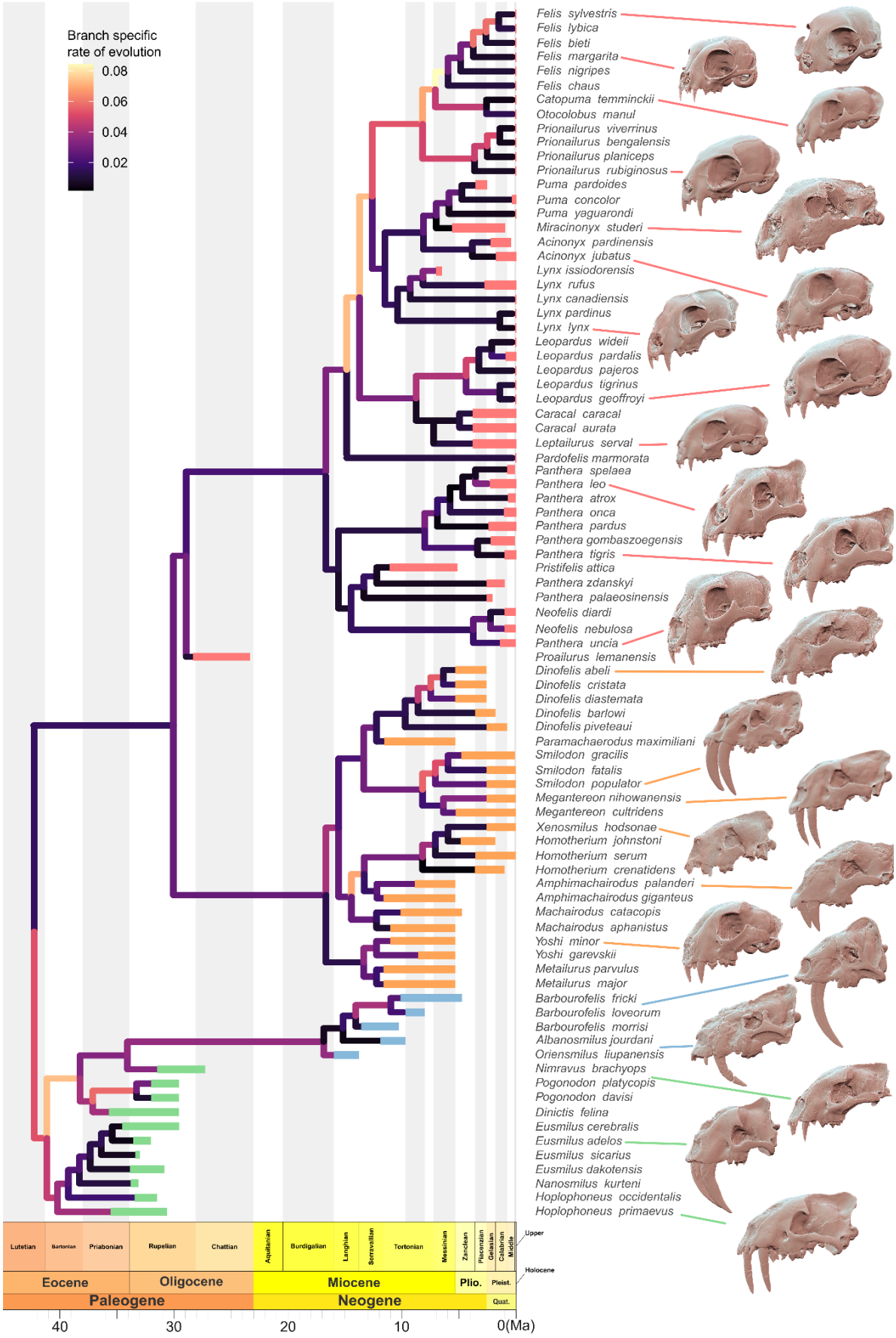

Figure S6: Branch specific rate of morphological evolution for the cranium obtained from the RRPhylo function. Related to Figure 5. Plio = Pliocene, Pleist = Pleistocene and Quat = Quaternary.

Landmark #	Description
1	Posterior base of the coronoid process, serving as the first anchorage point for the curve characterizing the shape of the coronoid process.
2	Posterior extent of the tooth row, second anchorage point for the curve characterizing the shape of the coronoid process.
3	Anterior extent and shape of the lower carnassial (labial).
4	Anterior extent and shape of the lower carnassial (lingual).
5	Anterior extent of the tooth row, first anchorage point for the curve characterizing the shape and size of the diastema
6	Posterior extent of the lower canine, second anchorage point for the curve characterizing the shape and size of the diastema
7	Anterior extent of the lower canine and the symphysis, first anchorage point for the curve characterizing the symphysial region and the ventral border of the mandibular corpus
8	Posterior extent of the angular process, second anchorage point for the curve characterizing the symphysial region and the ventral border of the mandibular corpus.
9	Labial extent of the mandibular condyle
10	Ventral extent of the mandibular condyle
11	Dorsal extent of the mandibular condyle

Table S1: Description of the fixed landmarks placed on the 99 mandibles. Related to STAR methods and Figure S1A.

Landmark #	Description
1	Most ventral point of the narial aperture, first anchorage point for the curve characterizing the dorsal profile of the skull (anterior) and first anchorage point for the curve characterizing the narial aperture.
2	Most dorsal point of the narial aperture at the junction of both nasal bones, , first anchorage point for the curve characterizing the narial aperture.
3	Most anterior point of the sagittal crest, second anchorage point for the curve characterizing the dorsal profile of the skull (anterior) and first anchorage point for the curve characterizing the dorsal profile of the skull (posterior)
4	Junction between the sagittal and nuchal crest, second anchorage point for the curve characterizing the dorsal profile of the skull (posterior) and first anchorage point for the curve characterizing the nuchal crest and zygomatic arc.
5	Most dorsal point of the post orbital process of the zygomatic, second anchorage point for the curve characterizing the nuchal crest and zygomatic arc and first anchorage point for the curve characterizing the orbit.
6	Most ventral point of the post orbital process of the frontal, second anchorage point for the curve characterizing the orbit.
7	Most anterior point of the junction between both premaxilla, first anchorage point for the curve characterizing the palate.
8	Most posterior point of the junction between both palatine, second anchorage point for the curve characterizing the palate.
9	Most posterior point of the intercondyloid notch
10	Most posterior point of the tooth row
11	Anterior extent of the upper carnassial
12	Most anterior extension of the tooth row.
13	Posterior extent of the upper canine.
14	Anterior extent of the upper canine.
15	Anterior extent of the palatine fissure.
16	Posterior extent of the palatine fissure.
17	Oval foramen
18	Most posterior extant of the suture between the palatine and the zygomatic.
19	Most ventral extant of the suture between both premaxillae.
20	Most dorsal extant of the infraorbital foramen.
21	Most ventral extant of the infraorbital foramen.
22	Most dorsal point of the foramen magnum.

Table S2: Description of the fixed landmarks placed on the 90 crania. Related to STAR methods and Figure S1B.

		Stayton 2015					
Pairs	**Bone**	**C2**	**p-value C2**	**C3**	**p-value C3**	**C4**	**p-value C4**
Yoshi minor – Acinonyx jubatus	**Cranium**	0.00185	**0.510**	**0.0042**	0.538	0.000001	0.510
	Mandible	**0.04805**	**0.037**	**0.1668**	**0.031**	**0.00003**	**0.035**
Hoplophoneus primaevus – Homotherium serum	**Cranium**	0	1	0	1	0	1
	Mandible	0.00468	0.471	0.013749	0.505	0.000003	0.484
Machairodus aphanistus – Panthera pardus	**Cranium**	0	1	0	1	0	1
	Mandible	0.00373	0.472	0.0150	0.474	0.000004	0.466
Machairodus aphanistus – Nimravus brachyops	**Cranium**	0	1	0	1	0	1
	Mandible	0	1	0	1	0	1
Megantereon nihowanensis– Eusmilus adelos	**Cranium**	0.24717	0.017	0.08849	0.052	0.0000235	0.019
	Mandible	0.03162	0.092	0.06839	0.214	0.0000185	0.106
Neofelis nebuolsa – Metailurus major	**Cranium**	0.005529	0.400	0.014008	0.444	0.0000046	0.417
	Mandible	0.014467	0.239	0.056397	0.233	0.000017	0.225
Neofelis nebulosa – Nimravus brachyops	**Cranium**	0.000123	0.612	0.000285	0.612	0	0.612
	Mandible	0.004514	0.547	0.013430	0.563	0.000003	0.556

Table S3: Results of Stayton convergence tests (C2, C3 and C4, see main document for C1 and comparison with Castiglione 2019). Related to Table 1, STAR methods and Figure S2 G-H.

Group tested	Structure	Phylogenetic signal (K)	p-value
Whole dataset	Cranium	0.2943	0.001
	Mandible	0.4943	0.001
Felidae	Cranium	0.3788	0.001
	Mandible	0.4656	0.001
Nimravidae	Cranium	0.5347	0.1129
	Mandible	0.7921	0.001
Felinae	Cranium	0.3552	0.043
	Mandible	0.4466	0.001
Machairodontinae	Cranium	0.565	0.001
	Mandible	0.4402	0.001
Nimravinae	Cranium	0.4888	0.2358
	Mandible	0.8095	0.002
Barbourofelinae	Cranium	0.6729	0.7033
	Mandible	0.7625	0.1149

Table S4: Phylogenetic signal on Procrustes coordinates for the cranium and mandible, for different clades. Related to STAR methods. Non-significant p-values are highlighted in grey.